Journal of Computer Networks and Communications

Emerging Topics in the Internet of Things

Lead Guest Editor: Huan Zhou
Guest Editors: Honglong Chen, En Wang, Behrouz Jedari, and Lei Mo

Emerging Topics in the Internet of Things

Journal of Computer Networks and Communications

Emerging Topics in the Internet of Things

Lead Guest Editor: Huan Zhou
Guest Editors: Honglong Chen, En Wang, Behrouz Jedari, and Lei Mo

Academic Editors

Contents

Hindawi
Journal of Computer Networks and Communications
Volume 2020, Article ID 2708357, 14 pages
https://doi.org/10.1155/2020/2708357

Review Article

A Node-Regulated Deflection Routing Framework for Contention Minimization

Bakhe Nleya[1] **and Andrew Mutsvangwa**[2]

[1]*Department of Electronic Engineering, DUT, Durban 4001, South Africa*
[2]*Faculty of Education, NWU, Potchefstroom, South Africa*

Correspondence should be addressed to Bakhe Nleya; bmnleya@gmail.com

Received 30 April 2019; Revised 9 December 2019; Accepted 28 December 2019; Published 8 June 2020

Guest Editor: En Wang

Optical Burst Switching (OBS) paradigm coupled with Dense Wavelength Division Multiplexing (DWDM) has become a practical candidate solution for the next-generation optical backbone networks. In its practical deployment only the edge nodes are provisioned with buffering capabilities, whereas all interior (core) nodes remain buffer-less. In that way the implementation becomes quite simple as well as cost effective as there will be no need for optical buffers in the interior. However, the buffer-less nature of the interior nodes makes such networks prone to data burst contention occurrences that lead to a degradation in overall network performance as a result of sporadic heavy burst losses. Such drawbacks can be partly countered by appropriately dimensioning available network resources and reactively by way of deflecting excess as well as contending data bursts to available least-cost alternate paths. However, the deflected data bursts (traffic) must not cause network performance degradations in the deflection routes. Because minimizing contention occurrences is key to provisioning a consistent Quality of Service (QoS), we therefore in this paper propose and analyze a framework (scheme) that seeks to intelligently deflect traffic in the core network such that QoS degradations caused by contention occurrences are minimized. This is by way of regulated deflection routing (rDr) in which neural network agents are utilized in reinforcing the deflection route choices at core nodes. The framework primarily relies on both reactive and proactive regulated deflection routing approaches in order to prevent or resolve data burst contentions. Simulation results show that the scheme does effectively improve overall network performance when compared with existing contention resolution approaches. Notably, the scheme minimizes burst losses, end-to-end delays, frequency of contention occurrences, and burst deflections.

1. Introduction

Dense Wavelength Division Multiplexing (DWDM) does support speeds in the terabit ranges in a single fiber; hence, it can adequately handle the massive amounts of heterogeneous data in present and future service networks. The terabit range speeds are primarily achieved by way of individually modulating several wavelengths before multiplexing them into a single fiber. In order to match the ultrahigh transmission speeds, the OBS paradigm was proposed as a candidate solution. OBS generally combines as well as represents a trade-off between other rival switching paradigms such as Optical Circuit Switching (OCS) and Optical Packet Switching (OPS). Whereas OCS may be relatively easy to implement, it however has a disadvantage of low network resources utilization and coarse granularity. On the other hand, OPS generally features excellent resources utilization as well as fine granularity even though it would be too costly to implement [1].

The edge (ingress and egress) nodes interface directly with user networks such as subscriber access, individual home metropolitan access rings, cloud centers, and smart grids. Core and edge nodes are mesh interconnected via DWDM links as illustrated in Figure 1. The primary functions of these two types of nodes are summarized in Figure 2. In practical operation, an ingress (edge) node assembles data packets destined for a common egress (edge) node into data bursts. Upon completion of a data burst

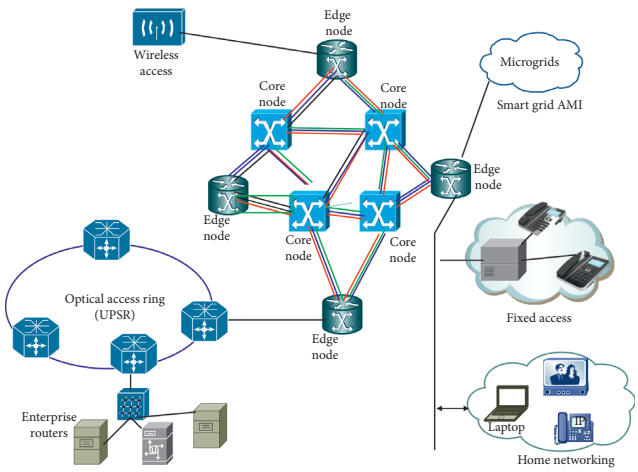

Figure 1: OBS backbone network [1].

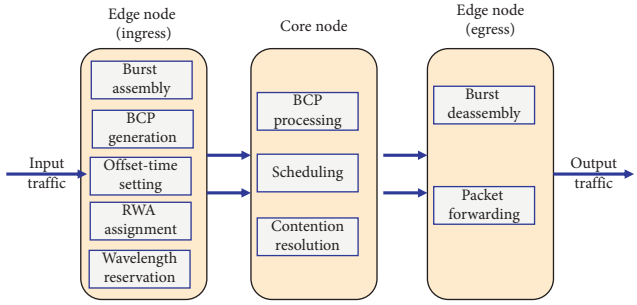

Figure 2: OBS network functional block diagram.

assembling, a signalling burst control packet (BCP) is generated and dispatched with an offset time ahead of the data burst. This will be delivered to the next (intermediate) node. The set offset time is critical in ensuring that required resources are configured at the next node prior to the data burst's arrival. Particularly, the offset timing is a time allowance for *processing* of the BCP at the next and subsequent nodes, reservation of a wavelength at the desired output port link, and preconfiguring the switching network with respect to the incoming and outgoing ports to be used [1]. The data burst later cuts through the node and shortly afterwards resources previously reserved for its switching are freed so that they can be utilized by other lightpath connection demands. The cut-through approach in handling the burst alleviates the necessity for any node buffering as this would otherwise escalate CAPEX/OPEX, as well as overall end-to-end delays for the data bursts. The momentary usage of resources enhances utilization as well as improves adaptability to highly heterogeneous traffic. When establishing an end-to-end lightpath connection, it is important to carefully select the set of candidate routing links as well as wavelengths at each ingress node so as to reduce the possibilities of data burst contentions occurring at subsequent nodes as a result of improper routing and wavelength assigning (RWA). In order to resolve any possible contention occurrences, limited extra resources in the form of wavelength converters (WCs) and optical (fiber) delay lines (FDLs) are provided. Once a data burst has successfully traversed the network, it will eventually be disassembled into individual packets which are then routed to their respective final destinations [1]. A key step in the design and deployment of OBS backbone networks is to optimize the limited available links as well as wavelengths such that a maximum possible number of lightpath connections can be established simultaneously. In essence, the RWA problem centers on establishing an end-to-end lightpath using a single wavelength. In so doing, this wavelength continuity constraint forbids the establishment of more than one lightpath using a particular wavelength concurrently on the same fiber link.

As core nodes do not directly interface with access networks, their primary functions are therefore restricted to BCP processing, scheduling, and contention resolution. Its functional components include input ports terminating each incoming fiber, output ports feeding to outgoing fiber links, a BCP processor, an optical cross-connect (OXC), wavelength converters (WCs), and FDLs. BCPs from ingress nodes are extracted at the input ports of intermediate nodes along the routing path then processed electronically by BCP processors. The offset timing relationship between a data burst and a BCP is illustrated as shown in Figure 3(a).

As was mentioned earlier, core nodes (Figure 3(b)) do not offer any buffering capabilities; thus, the data bursts cut through such nodes wholly in the optical domain. A performance drawback with regard to this being that some data bursts may be lost whenever contention occurs. The latter will always occur whenever more than one data burst destined for the same output port overlap in time and frequency.

Contention is regarded as a significant hindrance to the smooth operation of an OBS network as it often leads to significant burst losses and consequently QoS degradation. It arises when two or more data bursts utilizing an identical wavelength and destined for the same output port partially or wholly overlap in time. Both *reactive* and *proactive* contention resolution approaches are being implemented. Reactive contention resolution approaches attempt to resolve the contentions only after occurrence mainly in the core network, whereas proactive schemes are designed to avoid any contentions taking place in the network and effectively preventing any data burst losses.

Appropriate dimensioning of available network resources is regarded as a proactive contention prevention measure. Generally, it is relatively easier to implement proactive approaches at the ingress nodes routing the data on a carefully chosen optimal path to an intended destination coupled with optimal wavelength assigning to it. Network level performance metrics such as burst loss probability, end-to-end delays, and frequency of deflections serve as measures of optimality in the path and wavelength assigning.

Key reactive approaches include the use of limited available buffering in the form of FDLs, converting one of the contending data burst's wavelengths to any other available one using a WC, burst segmentation in which the overlapping sections of contending data bursts are discarded, *or* where one of the contending data bursts is deflected to any other available output port.

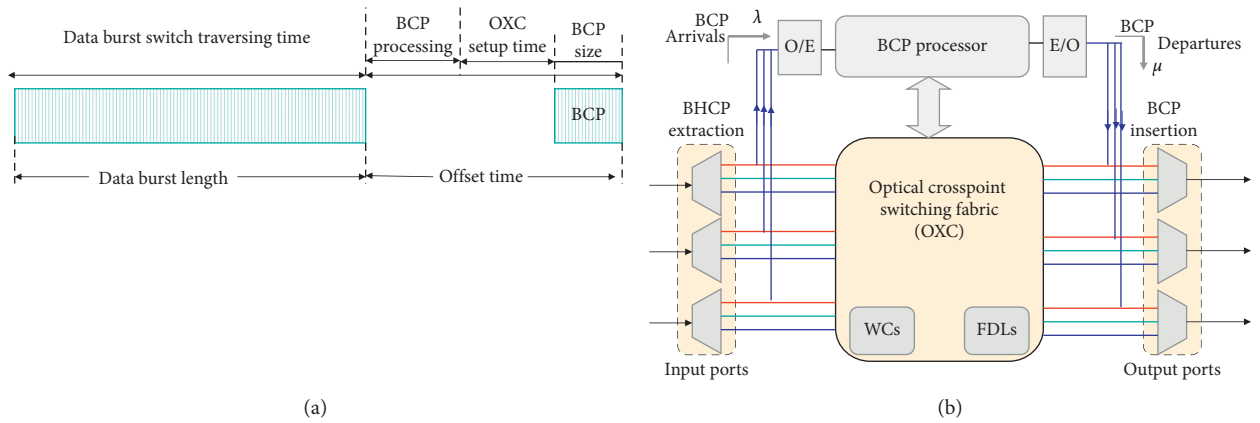

Figure 3: OBS core node.

2. Related Work on Contention Resolution

Accurately dimensioning network resources in relation to actual traffic volumes can be essential towards minimizing contention. However, not much work has been done towards accurately spelling out actual traffic flows throughout a given network. The authors in [2, 3] propose and evaluate an algorithm for obtaining a detailed end-to-end traffic matrix of a given network. Their proposed algorithm is based on fractal and cubic spline interpolation reconstruction approaches. The proposed algorithms will enable the attainment of detailed information about traffic flows on all active links of the network. However, both algorithms may still generate errors and hence this leads to inaccuracies in determining actual traffic flows. In a bid to further improve the reconstruction accuracy, the authors go on to propose the weighted geometric method whose simulation results [2] show relatively better accuracy in determining the network traffic flows. End-to-end traffic flow estimation based on measured source-destination flows is also explored in [3]. The proposed method herein, however, is deemed generally costly in implementation even though its measurement associated overheads are relatively low. In all cases, the various proposed methods attempt to acquire a better global view of the network's traffic flows. The traffic flow measurements obtained will enable network designers to accurately dimension all available network resources. In that way they alleviate possible congestion and contention occurrences since more effective RWA problem can be better resolved.

The RWA problem constitutes simultaneously setting up end-to-end lightpaths across the optical backbone transport network as well as routing and assigning a unique wavelength to each lightpath connection setup. In so doing, the wavelength continuity constraint must be maintained and at the same time designers are thriving to maximize the number of simultaneous connections with minimal network resources possible [4]. Once the network is operational, contentions will always occur in the intermediate nodes primarily because of their buffer-less nature. Extensive research work is focusing on minimizing the frequency of contention occurrences. The authors in [5] proposed and evaluated an algorithm that utilizes voids so as to minimize contentions as well as burst losses in interior nodes. The algorithm initially identifies all possible candidate void channels on which a data burst can be scheduled from before finally selecting one that maximizes the void utilization factor. Similarly, the authors in [6] propose a modified OBS paradigm that adapts assembled data burst sizes as a function of network traffic load. In this case when network loads are high, longer data bursts are assembled by the ingress nodes. Triangular estimator-based burst scheduling algorithms are proposed in [7]. All sections of the network that are currently prone to contention occurrences are identified as well as avoided when scheduling bursts. The authors in [8] studied adverse effects of deflection routing load balancing on general TCP performance. In their work, they suggest source ordering as a means of improving TCP throughput performance. Based on earlier findings, the authors in [9] extended the work by proposing a modified Horizon scheduling algorithm with minimum reordering effects (MHS-MOE). Artificial intelligence techniques are utilized to enhance the network's routing decisions by the authors in [10] who propose and analyze a Reinforcement Learning-Based Deflection Routing Algorithm (RLDRA). Their aim was to reduce data loss probabilities when the rate of contention occurrences at intermediate nodes surges significantly as a result of deflection traffic. Their scheme tries to control the count of authorized deflections for each burst to reduce the extra traffic generated by deflection routing. It also does not generate significant amounts of signalling and other computational overheads.

A multiclass preemptive scheduling-based scheme on deflection paths (routes) is proposed in [11] in which an attempt is made to improve general QoS of existing and future connections by implementing preemption policies on the onset of contention in the network. The proposed scheme's complexity is in the involvement of multitudes of parameters for determining and defining preemption probabilities and policies. Deflection routing in an anycast-based OBS grid is proposed by the authors in [12]. However, the accompanying proposed enhanced deflection routing algorithm does not appear to address or alleviate the contention problem satisfactorily. Fairness and data burst loss

owing to cascading constraint when bursts have longer hop count value in OBS networks is explored in [13]. The authors herein propose a preemptive scheduling technique for next-generation OBS networks in which newly arriving bursts with higher priority may preempt already scheduled ones when contention occurs.

It is on the strength of the earlier cited weakness that in this paper we propose a controllable deflection routing scheme which couples with a simple wavelength and routing assignment (WRA) algorithm to enhance overall network performance, by way of minimizing contention, wavelength congestion, and consequently bursts blocking probabilities. The scheme attempts as much as possible to deflect either of the contending bursts to paths that have been chosen based on the minimization of performance measures such as delay and blocking. It aims at controlling deflection traffic by way of selective path routing upon wavelength congestion onset. It is backed by a very simplified distributed RWA approach that ensures minimal contention in the primary (original) chosen route(s).

Summarily, the paper's contributions are as follows:

We propose a three-step approach to reducing contention occurrences in the core OBS network: (1) offset time regulation at burstification, (2) regulated deflection routing, and (3) neural network-based robust network state updating. Therefore, in this regard, the following steps are carried out:

(1) We describe a novel adjustable offset time coupled with a segmented burst assembly algorithm that regulates the offset timing such that extra delays are not incurred by traffic in the network. The algorithm suits both delay and non-delay-sensitive applications data.

(2) We develop a regulated deflection routing (rDr) scheme that is primarily concerned with the selection of the best-choice deflection routes at (from) each node when contentions have occurred, and deflection is necessitated. It is a proactive multipath neural network reinforced routing approach that seeks to avoid contentions occurring, as well as maintain load balancing in the overall network.

(3) For more accurate routing decision making by the node, we propose that neural network (NN)-based agents be incorporated to each routing node. The agents will form a distributed signalling network that periodically updates the entire network resources to routing tables. In that way, nodes can make better routing decisions. Each agent has a simple architecture; namely, it utilizes a single hidden as well as an associative learning algorithm to periodically update others regarding the state of network resources within the neighbourhood.

The rest of the paper is organized as follows:

In Section 2, we provide a brief description of deflection routing-based contention resolution in the core network. We introduce an adjustable offset timing burst assembly algorithm in Section 3. Neural network-based reinforcement learning is reviewed in Section 4, and in Section 5, we introduce a distributed regulated deflection routing framework. The same section discusses the NN-S algorithm. Section 6 is dedicated to evaluation, discussions, and conclusions.

3. Adjustable Offset Timing

Various traffic classes will always require some degree of QoS guarantees. During data burst assembling, QoS parameters such as jitter, blocking probabilities, and end-to-end delays can be minimized by reducing burstification delays as well as adaptively regulating the offset time [13]. Generally, burst assembly algorithms strive to strike balances between the rate at which BCPs are generated versus individual data burst sizes. The two are complimentary for moderate-to-high traffic loads in that maintaining huge data burst sizes during the assembly process would result in lesser numbers of BCPs generated per unit time. However, maintaining huge burst sizes will also lead to increased burstification delays when network traffic is low. Thus, the magnitude of offset timing chosen will directly influence end-to-end delays. Fixed offset timing gives extra time allowances for short data bursts but will be problematic for huge-sized bursts. In this paper, we adopt an adjustable offset timing algorithm during burst assembly whereby the actual offset time assigned is set as a function of an estimate of the current data burst size during its assembly [13, 14].

The adjustable offset time algorithm assumes the segmented burst assembly approach [15]. For a given source (s) to destination (d) node pair, the total end-to-end delay ($t_{d,s}$) is expressed as

$$t_{d,s} = t_{\text{ba}} + t_{\text{offset}} + h \times \left(t_{\text{proc}} + t_{\text{prop}}\right), \tag{1}$$

where t_{ba} is the burst assembly time at the ingress node, h is the hop count between s and d, t_{proc} is the processing and switching time at each node, and t_{prop} is the propagation time per hop distance.

Upon arrival of packets at an ingress node, the packets are assembled into class segments [15]; the maximum time delay tolerance of the packet class ($t_{\text{max\_class}}$) is set according to its QoS requirements.

$$t_{\text{max\_class}} \geq t_{d,s}. \tag{2}$$

If the $t_{\text{max(app)}}$ is less than the end-to-end delay time, $t_{d,s}$, then the offset time is calculated as

$$t_{\text{offset}} = \left(h \times t_{\text{prop}} + t_{\text{proc}}\right) - t_{\text{odv}}. \tag{3}$$

From (3), t_{odv} is an offset-time deducted value which is typically 90 nanoseconds [13].

The next burst assembly time (t_{out}) is computed from

$$t_{\text{out}} = \Delta t, \tag{4}$$

where

$$\Delta t = t_{\text{max\_class}} - t_{d,s}. \tag{5}$$

4. ANN Agents and Reinforcement Learning

Artificial Neural Networks (ANNs) are becoming a very popular tool for solving issues at operational level in networking.

The primary challenge in the use of ANN agents in this regard is for them to learn situation-to-action mappings in a particular network scenario and once the learning is successfully accomplished, the agent autonomously carries out the task. By availing appropriate data, an agent will quickly learn how to control a specific task in a networked environment. By leveraging complex statistical as well as mathematical tools, a given ANN set is capable of independently performing complex tasks that traditionally could only be solved by humans [16].

The adoption of ANN techniques in network routing was triggered by the unprecedented surge in network complexity. The large number of interdependent adjustable network system parameters such as modulation formats, coding schemes, routing configurations, and symbol rates contributes to overall network complexity. Figure 4 illustrates the principles of applying artificial intelligence in an OBS network. The agent routinely monitors the network (environment) for any state change(s) and actions to each of them accordingly. For every agent's action, the environment reciprocates with a reward signal. The agent in turn uses the reward signal for self-performance as well as on improving its subsequent decisions. For this reason, the agent requires a learning algorithm to enhance its interactions with the environment. It is expected to demonstrate intelligence capabilities by way of incorporating planning, reasoning, and knowledge. Because events in an OBS network are often nondeterministic, an agent must operate robustly under uncertainty. It should also make use of key decision-making algorithms so that they can maximize the expected utility. Practical OBS network environments mostly deal with uncertainties and hence the precision of an agent will depend on a multitude of interactions with the environment rather than a single isolated one. Learning is also a key issue that enables an agent to improve its accuracy on future decisions, based on previous experience. Learning will also help it to be adaptable to a changing environment. The learning phase is commonly referred to as machine learning (ML). The various learning algorithm categories include supervised learning, unsupervised learning, hybrid learning, and reinforced learning. In this section, we will elaborate more on reinforcement learning. In this case, the agent requires inputs such as jitter, tolerable network delays, and loss probabilities of various output ports (links) from the OBS network environment before responding accordingly with the most optimal link (path) choice towards a particular destination. The network eventually sends a positive or negative evaluative reinforcement feedback signal to the agent. The latter signal will be used by the agent to adjust its parameters accordingly so that it could improve on its future decisions regarding the same network aspect [17]. The reinforcement learning system also requires a strict policy so that the agent's behaviour can be regulated. It will also utilize reward function maps on each state–action pair of the environment to a numerical value which indicates the desirability of that state or the desirability of an action at that state [17, 18].

4.1. Extreme Learning Algorithm. In this subsection, we summarily describe an example ANN set learning algorithm called the extreme learning algorithm [10]. It facilitates the following key steps in order to arrive at a decision.

(i) Each ANN set accepts an input signal from its environment (the OBS network).

(ii) The input data set now traverses the entire set (via the hidden layer) and is eventually mapped to the output layer as an action.

(iii) The output of the ANN set is fed to the environment where the latter will evaluate it before subsequently responding to the NN set with a reinforcement signal r.

(iv) The NN set uses r to further improve on future decisions. This is achieved by modifying its weights accordingly.

We hereby take an example of estimating the blocking probability in an OBS network [19].

Th training set can be represented by a vector:

$$D = \left\{(x_k, p_k):\ x_k \in \mathfrak{R}^d,\ p_k \in \mathfrak{R}, k = 1, \ldots, N\right\}, \tag{6}$$

where x_k is the ANN input vector and y_k is a targeted output vector of k^{th} sample.

By assuming the ANN set comprises a single hidden layer, then

$$f_n(x) = \sum_{i=1}^{n} \beta_i g_i(x), \tag{7}$$

where g_i denotes the i^{th} hidden node's output, whereas β_i is the weight between the i^{th} hidden node and the output node.

The output function $g_i(x)$ of the i^{th} hidden node can thus be defined as

$$g_i(x) = \frac{1}{1 + e^{-\left(a_i^T x + b_i\right)}}, \tag{8}$$

where a_i is i^{th} hidden layer's input weight vector and β_i is the corresponding bias term.

If n hidden nodes are used for the approximation, then the mean square error (MSE) is

$$\varepsilon = \sum_{k=1}^{N} \left[p_k - \sum_{i=1}^{n} \beta_i g_i(x_k)\right]^2 = \left\| p - \sum_{i=1}^{n} \beta_i g_i \right\|_2^2. \tag{9}$$

In the above, $p = [p_1, \ldots, p_N]^T$ and $g_i = [g_i(x_i), \ldots, g_i(x_N)]^T$. At the n^{th} step, the training error is

$$\varepsilon_n = \left\| p - \sum_{i=1}^{n} \beta_i^2 g_i \right\|_2^2 = \left\| e_{n-1} - \beta_n g_n \right\|_2^2, \tag{10}$$

where $e_{n-1} = p - \sum_{i=1}^{n-1} \beta_i g_i$.

The output weight can thus be minimized using

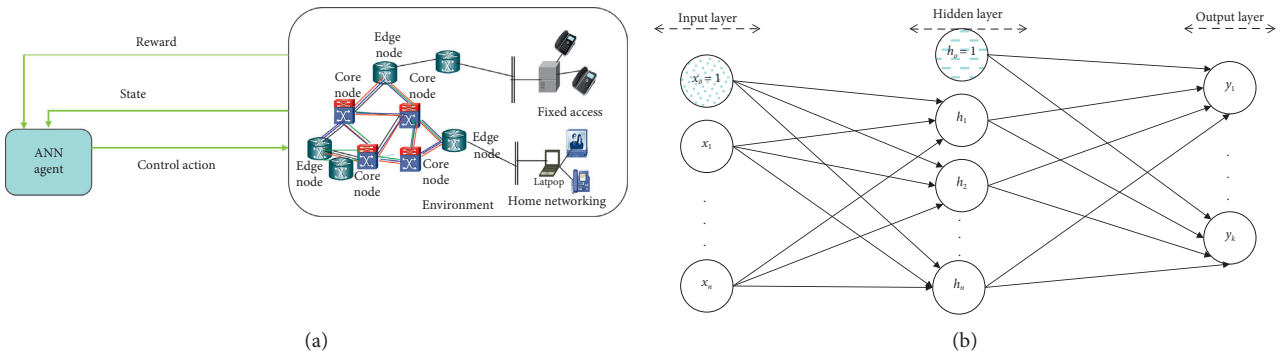

(a) (b)

Figure 4: Reinforcement learning principles.

$$\beta_n = \frac{e_{n-1}^T g_n}{\|g_n\|_2^2}. \tag{11}$$

5. Node-Regulated Deflection Routing Framework

We describe our proposed scheme as follows. Firstly, we discuss its principles followed by the learning scheme that would be used by the incorporated agent at a node in making key routing decisions. The ultimate objective of the scheme is to find an optimal route to deflect a contending burst if deflection routing is the only contention resolution scheme implemented in the particular network. The scheme thrives to ensure that each core node where contention is likely to occur learns to select an optimal deflection routing link(s) in terms of minimal blocking and delay with respect to the original route. In so doing, it thrives to minimize both signalling and computational overheads.

5.1. The Proposed Scheme. The proposed scheme's focus is on regulating selection of a deflection output port such that the chosen deflection route does not degrade the QoS of both the deflected bursts and existing traffic on the deflection link/path. We assume that should any two data bursts destined contend for the same output port, only one of them will be routed on the original path and the other will be deflected onto a selected least-cost deflection route. This is further illustrated by the queuing model in Figure 5(a). As defined in [20], deflection path server #1 queue represents a deflection path that offers a QoS nearing that of the original path.

A data burst will be deflected to path server #1 only if the controller buffer's capacity exceeds a threshold state q_1; otherwise, it will always be routed on the original path. Similarly, path server #2 would be the next-choice deflection route after the threshold exceeds q_2. Otherwise, in the absence of contention, the original path will always be preferred. The overall performance of a given link is time dependent; hence, Figure 5(b) illustrates these state changes for the two selected deflection paths. When busy, a selected deflection path exits the projected performance bounds at a rate α_j and conversely its performance improves at a rate β_j.

Summarily, the key steps are as follows:

(i) Sending node dispatches a BCP whose offset time is calculated according to (3) to the next intermediate node.

(ii) The BCP is processed upon its arrival at the next intermediate node. If desired primary route's output port and link wavelength are available, the burst will be accepted.

(iii) However, if contention or its imminence is detected, then the contention is resolved before the data bursts arrive as follows:

(a) If the current node is the ingress, its BCP is dropped and retransmission attempted at a later time.

(b) The other burst(s) can be either routed via the primary route, deflected to an alternate path, or worst case be discarded. This is done according to the set of rules in step iv as follows:

(iv) Data burst assigned to the original path: there are two or more contending bursts that have arrived and are all in transit. The controller buffer is in state $q < q_1$, and there are enough free wavelengths to accommodate all the contending bursts. Note that a link may have more than one fiber.

(a) deflected to path #1: the controller buffer is in state

$$q_1^* \le q \le q_2^*, \tag{12}$$

(b) deflected to path #2: the controller buffer is in state

$$q_2^* \le q \le q_N, \tag{13}$$

where q_N is the maximum possible aggregated deflection capacity on the two links.

Note that the threshold values q_1^* and q_2^* are set by taking into the key QoS metrics such as end-to-end delay and blocking.

5.2. Reinforcement Learning. We assume that the routing decisions pertaining to which deflection paths are determined by a routing agent. The Q-learning algorithm [21, 22]

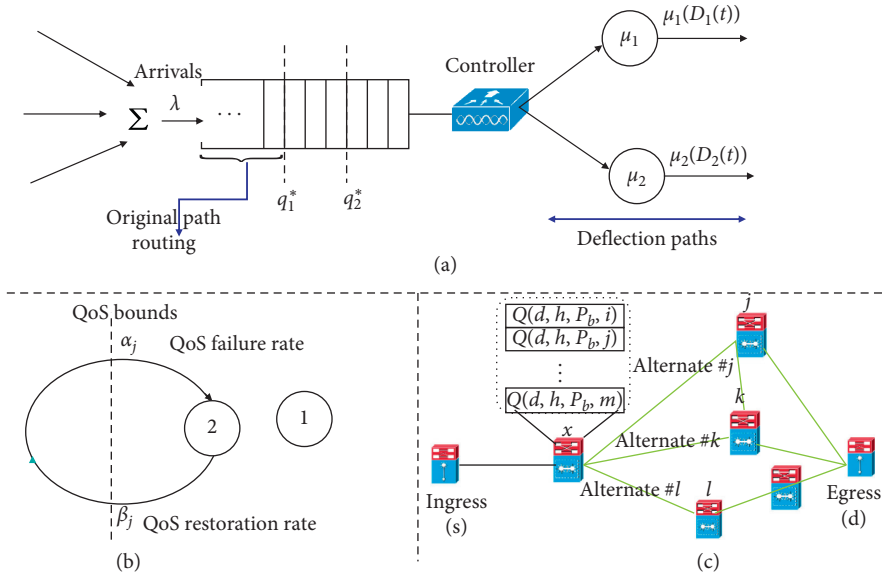

FIGURE 5: (a) Proposed scheme queuing model. (b) QoS state transitions. (c) Routing tables.

is adopted for this scheme. The Q-learning agent will gradually learn the best deflection route choice given a particular network state (s) after several trials of all possible actions (a) and by evaluating the corresponding reward $Q^{\pi}(s,a)$. The algorithm can be summarized in equation form as follows:

$$Q^{\pi}(s_t,a_t) \longleftarrow Q^{\pi}(s_t,a_t) + \alpha\left[r_{t+1} + \gamma_{a_{t+1}} \max Q^{\pi}(s_{t+1},a_{t+1}) - Q^{\pi}s_t,a_t\right], \tag{14}$$

where r is the discount rate, α is the learning speed, and s_t, a_t, and r_t are the state, action, and reward at a given time t, respectively.

Each core node's incorporated agent always learns the states of all links connected to the node and updates this information in the node's routing tables. In so doing, it stores Q-values for each outgoing/incoming link, each represented by a vector with entries such as blocking probability (P_b) and hop count (h). In addition, each entry is further indexed by the (destination, neighbouring node); (d,k), where d is the destination and k is the neighbouring node.

When it is desired to deflect a burst to a particular destination, the node will choose a link with the highest Q; that is,

$$y = \underset{z\in N(x),z\neq p}{\arg\max}\, Q_x^{\pi}(d,k,h,P_b), \tag{15}$$

where $Q_x^{\pi}(d,k,h,P_b)$ is the Q-values associated with neighbouring node z with respect to the destination (d) and $N(x)$ is the set of nodes (links) neighbouring x.

Subsequently, the node controller chooses the best two performing links to a particular destination, path #1, (Q_{1x}^{π}) and path#2, (Q_{2x}^{π}), where $Q_{1x}^{\pi} \geq Q_{2x}^{\pi}$. It then sets their threshold buffers q_1 and q_2.

After node x successfully deflects a data burst to a neighbouring node y, its agent receives a feedback signal $Q_y^{\pi}(d,z,h,P_b)$ that it uses to compute a reinforcement numerical as

$$f_{yx} = Q_y^{\pi}(d,z,h,P_b) \times Q_x^{\pi}(d,z,h,P_b). \tag{16}$$

Node x uses this value to update its deflection tables as

$$Q_x^{\pi}(d,y) \longleftarrow Q_y^{\pi}(d,y) = \frac{\alpha f_{yx}\left(1-B_{xy}\right)}{D_x(d,y)} - Q_x^{\pi}(d,y), \tag{17}$$

where B_{xy} is the burst lost probability along link $x \longleftrightarrow y$;

$$B_{xy} = \begin{cases} \dfrac{N_{\mathrm{drop}_{xy}}}{\mathrm{sent}_{xy} + N_{\mathrm{drop}_{xy}}}, & \text{if } \mathrm{sent}_{xy} + N_{\mathrm{drop}_{xy}} > 0, \\ 0, & \text{if } \mathrm{sent}_{xy} + N_{\mathrm{drop}_{xy}} = 0. \end{cases} \tag{18}$$

In (18), $N_{\mathrm{drop}_{xy}}$ is the total number of dropped bursts, while sent_{xy} is the total number of successfully transmitted bursts on the given link.

The deflection path loss probability from the point of deflection to destination d is

$$P_{xp} = 1 - \prod_{1\leq i\leq |P|-1} \left(1 - B_{h,h_{+1}}\right), \tag{19}$$

where $h_{1,\ldots,h|p|}$ is the number of remaining hops to the intended egress node.

5.3. Nodal Agent. In this section, we assume a feedforward single hidden ANN set for deflection routing. Its structure is shown in Figure 6.

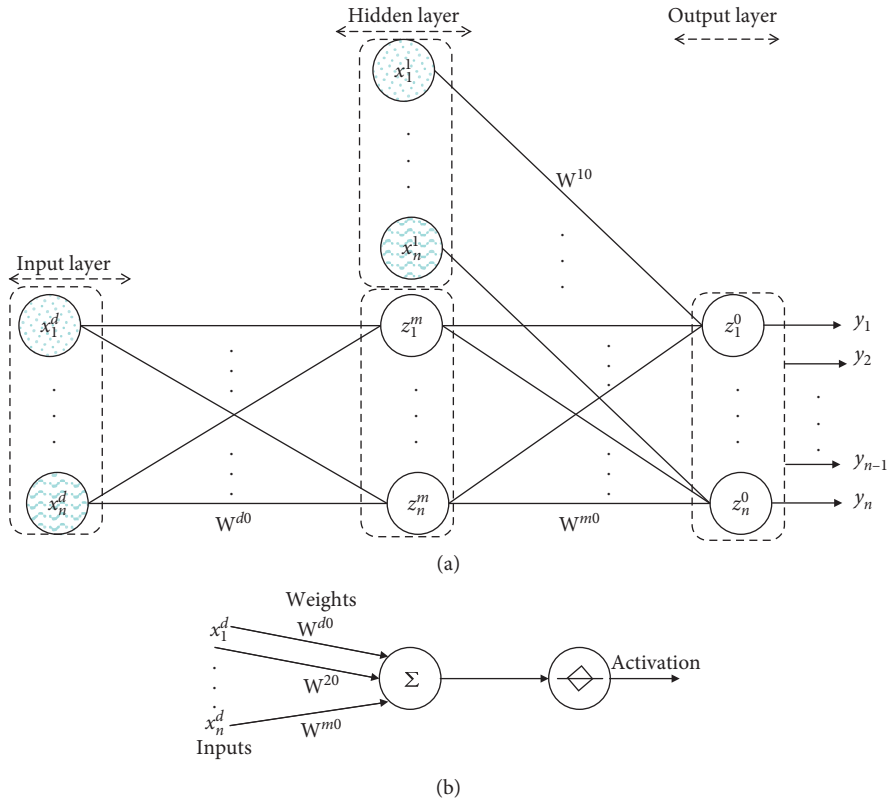

Figure 6: ANN for deflection routing.

It relies on its look-up table to store Q-values representing the states of all output links at a node to a particular egress node. This Q entry takes into account QoS metrics such as burst loss probability and remaining hope count as in (15). When a node receives BCPs and detects contention, its controller deflects one of the contending bursts to a neighbouring node with the highest Q-value with respect to intended destination. The agent has three layers, namely input, middle, and output layers. We assume that the OBS node has n outgoing ports. The input layer has two sublayers; namely,

$$\begin{aligned} \mathbf{I}^l &= \left[x_1^l, \ldots, x_n^l\right], \\ \mathrm{I}^d &= \left[x_d^l, \ldots, x_n^d\right]. \end{aligned} \tag{20}$$

If a port is blocked, then it is set to 1; otherwise, it is always set to 0.

The $\mathbf{I}^l$ input section's weights to the output layer can be expressed as a $n \times n$ matrix as follows:

$$W^{lo} = \begin{bmatrix} w_{11}^{lo} & 0 & \ldots & 0 \\ 0 & w_{22}^{lo} & \ldots & 0 \\ \vdots & & & \vdots \\ 0 & 0 & & w_{nm}^{lo} \end{bmatrix}. \tag{21}$$

If $Z^m = [z_1^m, \ldots, z_n^m]$ is a binary vector representing the middle layer, then it maps the input and the output layers using the matrix

$$W^{dm} = \begin{bmatrix} \omega_{11}^{dm} & \omega_{12}^{dm} & \ldots & \omega_{1n}^{dm} \\ \omega_{21}^{dm} & \omega_{22}^{dm} & \ldots & \omega_{2n}^{dm} \\ \vdots & \vdots & & \vdots \\ \omega_{n1}^{dm} & \omega_{n2}^{dm} & & \omega_{nm}^{dm} \end{bmatrix}, \tag{22}$$

$$W^{mo} = \begin{bmatrix} \omega_{11}^{mo} & \omega_{12}^{mo} & \ldots & \omega_{1n}^{mo} \\ \omega_{21}^{mo} & \omega_{22}^{mo} & \ldots & \omega_{2n}^{mo} \\ \vdots & \vdots & & \vdots \\ \omega_{n1}^{mo} & \omega_{n2}^{mo} & & \omega_{nn}^{mo} \end{bmatrix}. \tag{23}$$

The matrices given in (21) and (22) reflect deflection route preferences and are continuously updated and new reinforcement signals are received from the OBS network (environment).

Therefore, for any given $h \times k$ matrix $\mathbf{Q}$, a Bernoulli semilinear operator $\Phi(\mathbf{Q})$ can be defined as

$$\Phi(\mathbf{Q}) = \begin{bmatrix} \dfrac{1}{1+e^{q_{11}}} & \cdots & \dfrac{1}{1+e^{q_{1k}}} \\ \vdots & \vdots & \vdots \\ \dfrac{1}{1+e^{q_{h1}}} & \cdots & \dfrac{1}{1+e^{q_{hk}}} \end{bmatrix}. \tag{24}$$

In each decision making, a probability vector

$$\mathbf{P}^m = \lfloor\, p_1^m \;\; \cdots \;\; p_n^m \,\rfloor, \tag{25}$$

is computed using the Bernoulli semilinear operator as

$$\mathbf{P}^m = \Phi\left(\mathbf{I}^d \times \mathbf{W}^{mo}\right). \tag{26}$$

Each element $x_k^m \in \mathbf{Z}^m$ is calculated as follows:

$$x_k^m = \begin{cases} 0, & \text{if } p_k^m < 0.5, \\ U(0,1), & \text{if } p_k^m = 0.5, \\ 1, & \text{if } p_k^m > 0.5, \end{cases} \tag{27}$$

where $U(0,1)$ assumes 0 or 1 from a uniform distribution.

We further let $1 \times 2n$ row vector $\mathbf{I}^o = [\mathbf{I}^l \mathbf{Z}^m]$ represent an input to the output layer $\mathbf{Z}^o$.

The $n \times 2n$ matrix $\mathbf{W}^o = \left\lfloor \mathbf{W}^{lo} \mathbf{W}^{mo} \right\rfloor$ represents the weight matrix of the output layer $\mathbf{Z}^o$. The probability vector is calculated as

$$\mathbf{P}^o = \left\lfloor p_1^0, \ldots, p_n^0 \right\rfloor = \Phi\left(\mathbf{I}^o \times (\mathbf{W}^o)^T\right). \tag{28}$$

Finally, the binary output vector $\mathbf{Z}^o = [z_1^o, \ldots, z_n^0]$ can now be calculated. Indices of 1s appearing in the output vector indicate availability of that output for deflection.

6. Simulation Results and Analysis

In this section, we evaluate the performance of the proposed rDr scheme by way of simulation. The simulation focuses on QoS metrics such as loss probability, frequency of contentions occurring, number of deflections, mean burst end-to-end latencies, number of deflections, and deflection path lengths (measured in hops).

Our simulations are carried out on an online NS-2 simulator [23], together with OBS modules that are implementable in the same simulator [24]. Only the 15-node mesh topology network shown in Figure 7 was considered for the simulations. Each fiber link terminates with a standard port on either end and is bidirectional and all fibers have equal numbers of wavelengths. Only the edge nodes on the network can be ingress (source) and egress (destination) points for the traffic, while the rest route traffic. The sources and destination pairs are randomly chosen from among the designated edge nodes. The traffic load normalized to the maximum link capacities, i.e., the ratio of incident traffic to a node and the aggregated capacities of all the wavelengths constituting the link.

The dynamic segmented burst assembly approach coupled with adjustable offset timing algorithm as described in Section 2 is assumed. For the sake clarity, the dynamic segmented burst assembly algorithm's model is illustrated in Figure 8, which is presented in detail in [15]. Two traffic type streams whose arrival rates are λ_1 (high priority) and λ_2 (low priority) are considered. The assembly approach is summarized as follows:

(i) The buffer sizes are H_1 (high priority) and H_2 (low priority)

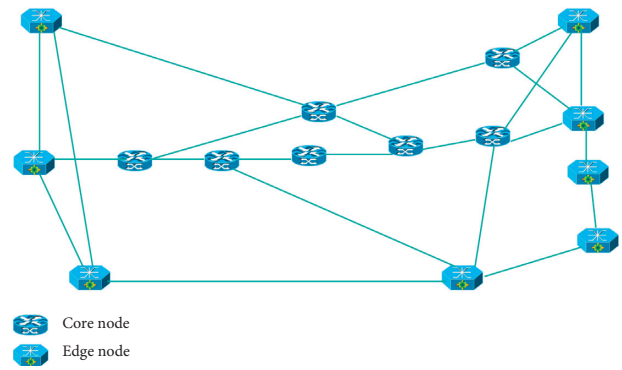

Figure 7: NSFNET topology network.

(ii) A new HP segment arrival will always be accepted in the HP buffer provided it is not full; otherwise, it is discarded

(iii) If upon arrival of a new LP segment, the total number of segments in the LP buffer is i, $i < H_2$ and the number of segments in the HP buffer is j, $j < H_1$, the LP segment jumps to the HP buffer with probability $p_i(j)$ and will now be served as a HP segment; as such an arriving LP segment joins the LP buffer with probability $1 - p_i(j)$

(iv) A new LP segment arrival will be discarded if the HP and LP buffers are in states H_1 and H_2, respectively

(v) A new LP segment arrival finding the LP buffer in state (H_2), but the HP buffer in state j, $j < H_1$ will be admitted to the latter with probability $p_{H_2}(j)$, or else be discarded with probability $1 - p_{H_2}(j)$

In our performance evaluations, we use both delay-sensitive and non-delay-sensitive sources. Since all networks that employ (adopt) deflection routing may suffer from insufficient offset timing problem, we first simulate the end-to-end delays as well as burst loss ratios of the proposed adjustable offset timing scheme coupled with segmented burstification. Here we restrict ourselves to the HP class (delay-sensitive traffic type) as the two QoS parameters (blocking and end-to-end delay) are relatively critical to this class than the LP one. Note that when LP segments (bursts) are lost, they can always be retransmitted.

Each link has one GHz bandwidth and BCP processing time at each intermediate node is 1.5 μ secs. The propagation delay averages 1 μ sec on each hop. Each segment size is 50 packets and that of the segmented burst is 4000 kB. Only HP class data segments are generated and their arrival at the burstification buffers follows a Poisson distribution. We also set three different values for the maximum burst transfer delay ($t_{d,s}$) to 90 μ secs, 120 μ secs, and 135 μ secs. The traffic intensities will be varied from low to high. Shown in Figure 9 are the average end-to-end delays for the high-class segments (or packets) for three different values of maximum burst transfer delay limits. In this case, the offset time is computed according to (3) subject to (2).

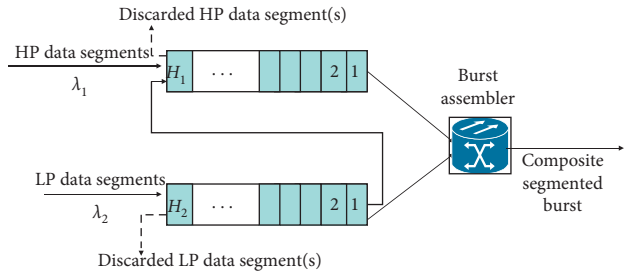

Figure 8: Dynamic segmented burst assembly approach.

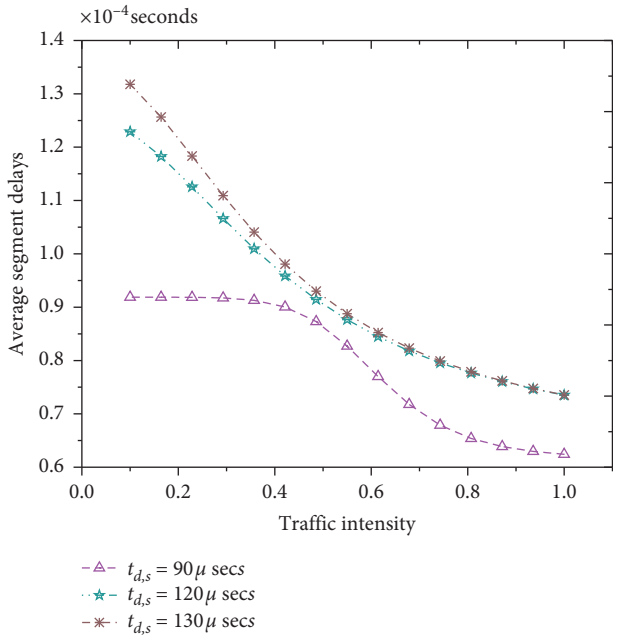

Figure 9: Average segment (packet) delays end to end.

As can be observed for low traffic levels, the average delay is determined by the preset maximum burst transfer delay values which are 90, 120, and 130 microseconds, respectively. The plotted results overall demonstrate that the Segmented Burst assembly approach coupled with the offset time approach will significantly reduce the end-to-end delays incurred by the HP traffic. It is also observed that for low traffic intensities, setting the maximum end-to-end delay ($t_{d,s}$) to a low value yields overall less delays. This is because the segmented bursts are dispatched for scheduling without waiting for the completion of burst aggregation. At high traffic intensities, the aggregation time is still less than the maximum delay.

We now turn to the burst loss ratio, in which we compare the proposed adjustable offset time scheme to the conventional OBS (where the offset time is fixed). The simulation results are shown in Figure 10. For traffic intensities ranging from zero to about 0.5, the two approaches perform comparably the same. However, the proposed adjustable offset approach still performs relatively better at peak traffic intensities. This is because as traffic increases, the conventional offset time scheme generates more bursts and this leads to more contentions (leading to burst losses). On the other hand, the proposed scheme generates relatively fewer but longer bursts and this coupled with adjustable offset timing still results in fewer contentions as well as sufficient burst processing times.

We further evaluate the performance of the proposed rDr scheme with respect to the number of deflections, burst loss probabilities, and average end-to-end delays. In so doing, we compare the scheme to existing similar schemes such as the following:

(i) Shortest Path Deflection Routing (SPDR) which was proposed in [25] is generally considered as the conventional OBS deflection scheme. We however place a restriction on the number of deflections by a single burst to three. This is to prevent endless looping in the OBS network which otherwise may lead to more contentions as well as other network performance degradations.

(ii) The Reinforcement Learning-Based Alternative approach (RLAR) which is analysed in [25] is basically based on Q–reinforcement learning NN nodes at each core node, and it allows data bursts to be routed on any available link rather than on a shortest path link from source to intended destination. It resolves contention by merely discarding one of the contending data bursts.

(iii) The Reinforced Learning-Based Deflection Routing Scheme (RLDRS) proposed in [26] is a proactive-based algorithm that capitalizes on what a NN set has learnt from the network by choosing a link with maximum Q in the deflection routing table to forward an incident contending burst.

Our blocking probability ranges are from $P_b = 1 \times 10^{-6}$ to about $P_b = 1 \times 10^{-3}$ and so our training data set is generated according to these desired ranges. Similarly, the same was done for the end-to-end delays which should be within the desired QoS ranges.

In our simulation, arrival processes of data bursts to a node are assumed to be Poisson-distributed, and hence service times are exponentially distributed. Listed in Table 1 are some of the key parameters for the simulation as well as training model. The data sets used are provided in Table 2.

During the actual training phase, the NN set was learned as outlined in IV; that is, initially we set the residual error value $e_0 = p$. We also set the number of hidden nodes to zero, i.e., $n = 0$. Further, we define the termination condition e. We then progressively increase the number of hidden nodes n as long as the following conditions are not violated:

$n \le n_{\max}$ and $((\varepsilon_{n-1} - \varepsilon_n)/\varepsilon_{n-1}) > 0$. Further, we go on to add an additional $g_n(.)$ hidden to the network where, (a_n, b_n) are randomly generated. We then compute the new weight β_n.

$$\beta_n = \frac{e_{n-1}^T e_n}{\|g_n\|_2^2}, \tag{29}$$

and further,

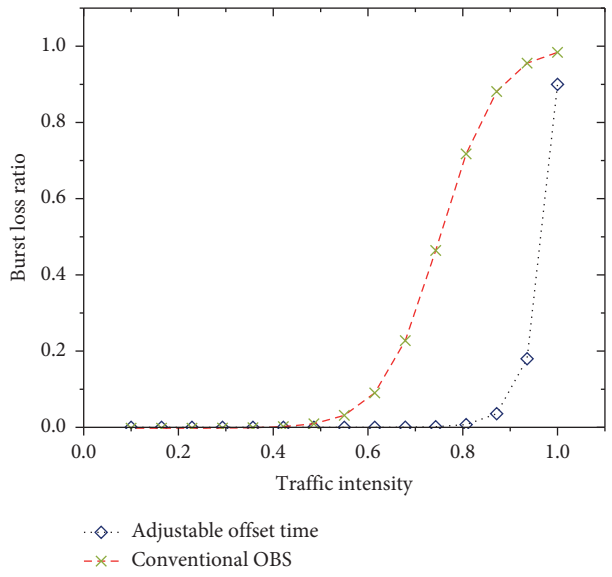

Figure 10: Burst loss ratio due to contentions.

Table 1: Input parameters to the NN set.

Parameter	Definition
N_λ	Capacity of link in, i.e., number of wavelengths
$\overline{\rho}_{s,d}$	Average normalized traffic load in s,d pair
$\Delta\overline{\rho}_{d,s}$	Difference between maximum and minimum traffic loads on a s,d pair and is uniformly distributed
$\overline{h}$	Mean path length
CR	Route traffic concentration
α	NN set learning rate

Table 2: Data sets.

Class	Lower bound		Upper bound	
	P_b	$t_{d,s}\,(\mu s)$	P_b	$t_{d,s}\,(\mu s)$
I	1×10^{-6}	750	1×10^{-4}	1000
II	1×10^{-4}	1001	5×10^{-5}	2000
III	5×10^{-2}	2001	0.25	5000

$$e_n = e_{n-1} - \beta_n^{g_n}. \tag{30}$$

Once training is accomplished, simulations of various OBS network QoS metrics are obtained. In all cases, several random assignments of node destination pairs are assigned and then results obtained are averaged. Figure 11 shows the overall mean end-to-end delays experienced by the data bursts as they traverse the network. As can be observed in this figure, the SPDR outperforms all other algorithms since it is solely based on establishing shortest path deflection routes to an intended destination. The rDr is outperformed by the other three since it does not necessarily utilize the shortest paths and the burstification approach does regulate the magnitude of the offset times.

The end-to-end delay is acceptable for medium-sized networks as well as for most application types that do not impose stringent delay requirements. Because unresolved contentions may lead to burst losses, we proceed to compare the four schemes' performance with regard to blocking.

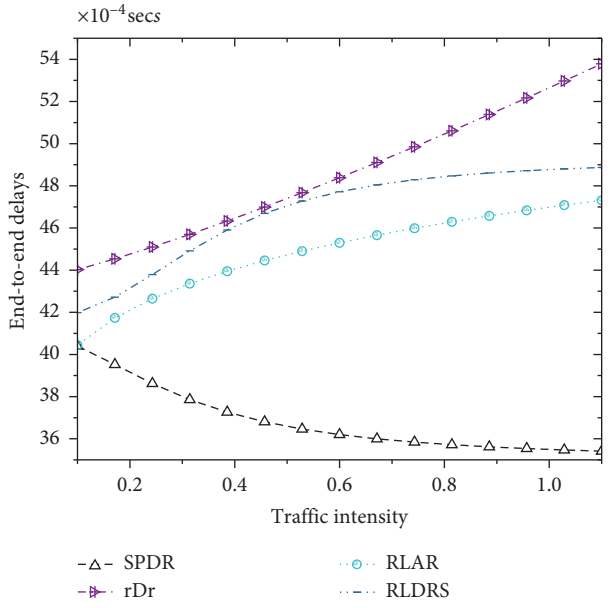

Figure 11: Average end-to-end burst delays.

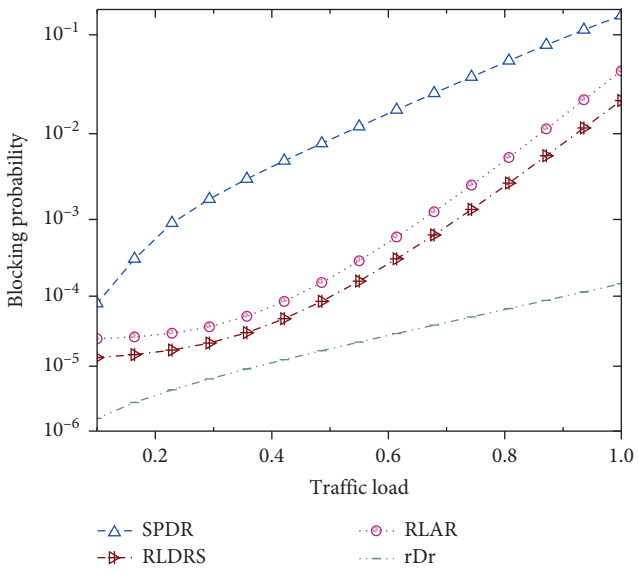

Figure 12: Blocking probability versus traffic load.

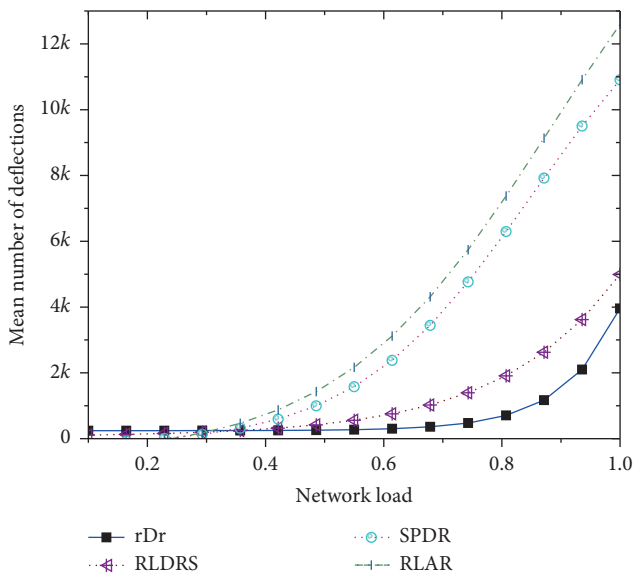

Figure 13: Mean number of deflections versus traffic load.

Shown in Figure 12 are the results obtained when the traffic load was varied from low to moderate and eventually to high (100% loading). It can be deduced from the graph that the rDr appears to be outperforming the other three algorithms at all levels of traffic in terms of burst blocking. This is partly attributed to the fact that the deflection paths in rDr are chosen from among the best two candidate routes and this still leaves the rest of the network unaffected by deflection traffic. The careful choice of deflection routes in rDr implies that any adverse effects of deflection routing are minimized. This can be easily observed in Figure 13 where we plot the mean number of deflections as the network load is increased gradually to maximum.

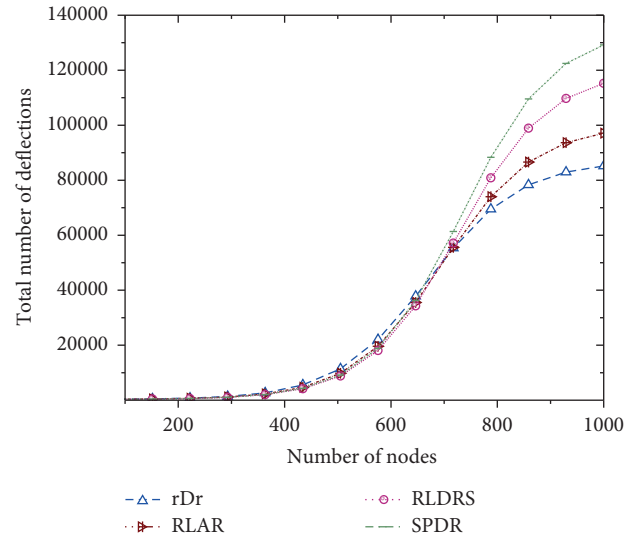

Figure 14: Total number of deflections versus number of nodes.

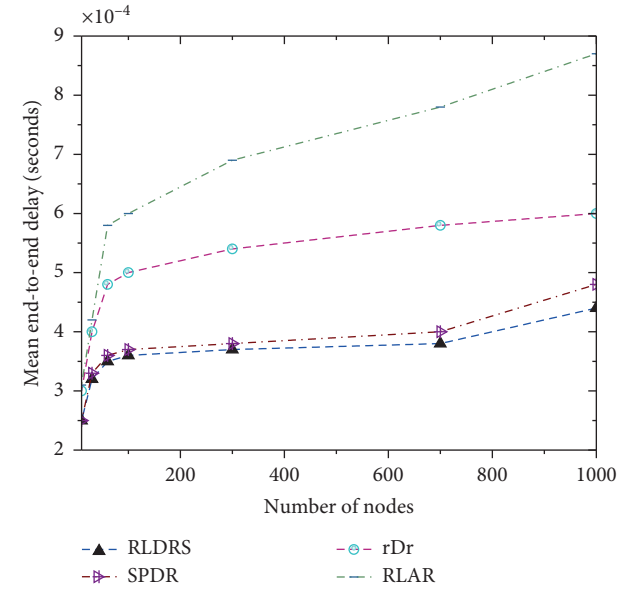

Figure 15: Mean end-to-end delays as function of network size.

It is noted that for the proposed scheme, the number of deflections only starts to surge when the network load exceeds 0.77.

The BRITE network topology generator [27] is further used to generate network topologies with varying numbers of nodes up to a maximum of 1000. With this generator, an edge that connects nodes v and u exists with probability:

$$\text{Prob}(\{v,u\}) = \beta e^{-(d(v,u)/L\delta)}. \quad (31)$$

In (28), $d(u,v)$ is the distance between nodes v and u; L is the maximum link distance between two nodes, whereas β and δ are parameters that take values in the range $[0,1]$.

Figure 14 shows the performance of the 4 algorithms in terms of deflections. The rDr outperforms the rest as the

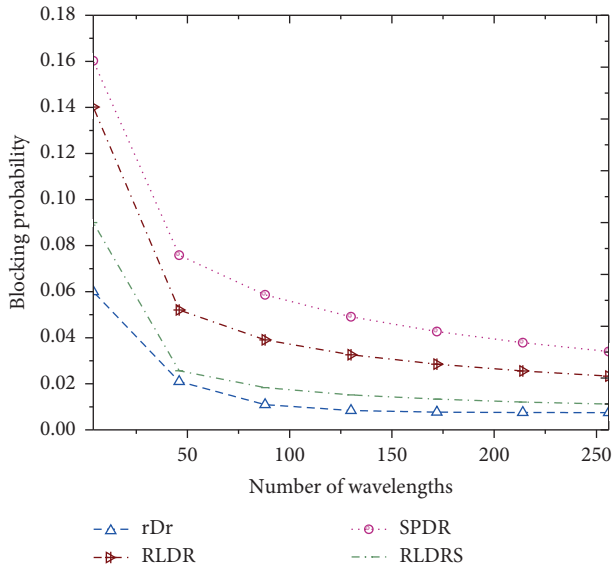

Figure 16: Blocking probabilities as a function of number of wavelengths.

network is expanded to a maximum of 1000 nodes. However, even though the blocking probabilities of the rDr algorithm is lower since the bursts are deflected less frequently, this is at the expense of having to incur larger end-to-end delays as the algorithm tends to select longer paths as indicated by the results plotted in Figure 15. RLDRS and the SPDR algorithms always opt for the shortest paths when deflecting contending bursts. However, the probability of further encountering both contentions as well as congestion is relatively higher because the majority of current day routing protocols always choose to route data via shorter routes.

Note that even though reduced burst deflection reduces the burst-loss probability, it still introduces excess traffic load in the network sections previously underloaded. We further extended our study to investigating the effects of increasing the number of wavelengths on the end-to-end delays. We had to fix the traffic load to about 60% and varied the traffic number of active wavelengths on each link from 4 to about 25.

It is observed from Figure 16 that rDr, RLDRS, and RLAR algorithms reduced blocking probabilities as the number of wavelengths is increased. However, this leads to increases in end-to-end delays.

7. Conclusions

Deflection routing being a key contention resolution scheme in present day OBS network motivated us into proposing and analysing a reinforcement learning-based regulated deflection routing (rDr) scheme. For periodic updating of the entire network resources, we propose an artificial neural network signalling algorithm (ANN-S) that utilizes a single hidden layer as well as an associative learning algorithm to periodically update routing tables so that nodes can make better routing decisions. Furthermore, we proposed coupling the use of the adjustable offset timing approach with segmented burst assembling to enhance QoS performance of the overall network, in particular, with regard to accommodating delay-sensitive applications. The reinforced learning is implemented in the NS-3 platform available online. We tested reinforcement learning-based regulated deflection routing algorithm on the same platform. We also utilized the National Science Foundation (NSF) network topology and random graphs that consisted in varying the number of nodes up to a maximum of 1000 for further simulations. Ultimately, we compared the rDr scheme to existing similar OBS deflection schemes such as Shortest Path Deflection Routing (SPDR), the Reinforcement Learning-Based Alternative Approach (RLAR) [19], and the Reinforced Learning-Based Deflection Routing Scheme (RLDRS) proposed in [20]. Key notable QoS metrics of interest during the simulations were burst loss probabilities, end-to-end delays, and the number and frequency of deflections.

Our simulation results showed that overall the rDr scheme by comparison significantly and effectively reduces loss probability even though at a cost of negligible increases in the end-to-end mean delays. Our further investigation will include increasing the number of traffic classes in an attempt to balance between the frequencies of contentions that ultimately contribute to burst loss probabilities versus end-to-end latencies especially during peak traffic periods. In [28], the authors propose and discuss methods related to QoS evaluation with regard to selecting an energy efficient network. The metrics taken into account also include energy cost, network cost, end-to-end delays (latency), and bandwidth. In our future work, we will incorporate the energy cost metric when selecting a "least cost route" so as to guarantee an energy-efficient network design [29]. With regard to proper dimensioning of the available network resources, we will further take into account the effect of access network traffic behaviours.

Conflicts of Interest

The authors declare that they have no conflicts of interest regarding the publication of this paper.

References

[1] T. M. Hirata and T. Takine, "Dynamic burst discarding scheme for deflection routing in optical burst switching networks," *Optical Switching and Networking*, vol. 4, no. 2, pp. 106–120, 2007.

[2] L. Huo, D. Jiang, X. Zhu, Y. Wang, Z. Lv, and S. Singh, "Ä SDN based fine grained measurement and modelling approach to vehicular communication network traffic," *International Journal of Communication Systems*, 2019.

[3] L. Nie, D. Jiang, and L. Guo, "A comprehensive sensing based approach to end to end network traffic reconstruction utilizing partial measured origin-desination flows," *Transactions on Emerging Telecommunications Technologies*, vol. 26, no. 18, pp. 1108–1117, 2015.

[4] S. S. Chawathe, "Analysis of burst header packets in optical burst switching networks," in *Proceedings of the 2018 IEEE*

17th International Symposium on Network Computing and Applications (NCA), Cambridge, MA, USA, November 2018.

[5] M. Nandi, A. Turuk, D. Puthal, and S. Dutta, "Best fit void filling algorithm in optical burst switching networks," in *Proceedings of the Second International Conference on Emerging Trends in Engineering and Technology, ICETET-09*, pp. 609–614, Nagpur, Maharashtra, India, 2009.

[6] T. Bonald, R. Indre, and S. Oueslati, "Adaptive optical burst switching," in *Proceedings of the 23rd International Teletraffic Congress*, pp. 150–157, San Francisco, CA, USA, September 2011.

[7] C. Papazoglou, P. G. Sarigiannidis, G. I. Papadimitriou, A. S. Pomportsis, S. Andreas, and S. Pomportsis, "The use of a triangular estimator to improve scheduling in optical burst switched networks," *International Journal of Communication Systems*, vol. 23, no. 2, pp. 187–203, 2010.

[8] B. Komatireddy, D. Chandran, and V. M. Vokkarane, "TCP-aware load-balanced routing in optical burst-switched (OBS) networks," in *Proceedings of the Optical Fiber Communication Conference and Exposition and The National Fiber Optic Engineers Conference, OSA Technical Digest Series (CD) (Optical Society of America, 2007), paper OWC6*, New York, NT, USA, 2007.

[9] K. Ramantas, T. R. Varga, J. C. Guerri, and K. Vlachos, "A preemptive scheduling scheme for flexible QoS provisioning in OBS networks," in *Proceedings of the IEEE Sixth International Conference on Broadband Communications, Networks, and System (BROADNETS 2009)*, pp. 1–6, Faro, Portugal, 2009.

[10] A. H. Belbekkouche and M. Gendreau, "A reinforcement learning-based deflection routing scheme for buffer-less OBS networks," in *Proceedings of the IEEE Global Telecommunications Conference, (IEEE GLOBECOM'08)*, pp. 1–6, New Orleans, LO, USA, 2008.

[11] G. Gurel, O. Alparslan, and E. Karasan, "nOBS: an ns2 based simulation tool for performance evaluation of TCP traffic in OBS networks," *Annals of Telecommunications*, vol. 62, no. 5-6, pp. 618–632, 2007.

[12] M. De Leenheer, J. Buysse, C. Develder, B. Dhoedt, and P. Demeester, "Deflection routing in anycast-based OBS Grids," in *Proceedings of the IEEE International Workshop on Optical Workshop on Optical Burst/Packet Switching*, Nagpur, Maharashtra, India, 2009.

[13] C. Xiaoyuan, X. H. W. Jian, and L. Jintong, "An adaptive offset time scheme in obs network," in *Proceedings of the 2008 7th International Conference on Optical Internet*, Tokyo, Japan, 2008.

[14] T. Mikoshi and T. Takenaka, "Improvement of burst transmission delay using offset time for burst assembly in optical burt switching," in *Proceedings of the7th Asia-Pacific Symposium on Information and Telecommunication Technologies*, pp. 13–18, Maldives, South Asia, 2008.

[15] H. Sibanda and B. Nleya, "Model analysis of dynamic priority segmented burstification and deflection routing," in *Proceedings of the 2017 IEEE AFRICON*, Cape Town, South Africa, September 2017.

[16] A. F. L. Calderon, E. J. V. Porras, and O. J. S. Parra, "Predicting traffic through artificial neural networks," *Contemporary Engineering Sciences*, vol. 10, no. 24, pp. 1195–1209, 2017.

[17] J. Mata, I. Miguel, R. J. Durán et al., "Artificial intelligence (AI) methods in optical networks: a comprehensive survey," *Optical Switching and Networking*, vol. 28, pp. 43–57, 2018.

[18] C.-S. Leung, W. Y. Wan, and R. Feng, "A regularizer approach for RBF networks under the concurrent weight failure situation," *IEEE Transactions on Neural Networks and Learning Systems*, vol. 28, no. 6, pp. 1360–1372, 2017.

[19] J. Tang, C. Deng, and G.-B. Huang, "Extreme learning machine for multilayer perceptron," *IEEE Transactions on Neural Networks and Learning Systems*, vol. 27, no. 4, pp. 809–821, 2016.

[20] P. Z. Khumalo and B. Nleya, "A controllable deflection routing and wavelength assignment algorithm in OBS networks," in *Proceedings of the International Conference on Intelligent & Innovative Computing Applications (ICONIC)*, Plaine Magnien, Mauritius, December, 2018.

[21] G.-B. Huang, Q.-Y. Zhu, and C.-K. Siew, "Extreme learning machine: theory and applications," *Neurocomputing*, vol. 70, no. 1–3, pp. 489–501, 2006.

[22] S. Haerei and L. Trajikovic, "Intelligent deflection routing in bufferless networks," *IEEE Transactions on Cybernetics*, vol. 45, no. 2, pp. 316–327, 2015.

[23] NS-Simulator, http://www.isi.edu/nsnam/ns.

[24] S. Gowda, R. K. Shenai, K. M. Sivalingam, and H. C. Cankaya, "Performance evaluation of TCP over optical burst-switched (OBS) WDM networks," in *Proceedings of IEEE International Conference on Communications, 2003. ICC '03*, vol. 2, pp. 1433–1437, Anchorage, AK, USA, May 2003.

[25] T. Coutelen, H. Elbiaze, B. Jaumard, and A. Metnani, "Impact of network topology and traffic load balancing on deflection routing efficiency," in *Proceedings of IASTED OCSN*, Banff, Canada, 2005.

[26] A. H. M. G. Belbekkouche, "A reinforcement learning- based deflection routing scheme for buffer-less OBS networks," in *Proceedings of IEEE GLOBECOM*, New Orleans, LO, USA, 2008.

[27] BRITE, 2014, http://www.cs.bu.edu/brite/.

[28] D. Jing, L. Huo, Z. Lv, H. Song, and W. Qin, "A joint multi criteria utility based network selection approach for vehicle to infrastructure networking," *IEEE Transactions on Intelligent Transporattion Systems*, vol. 19, no. 10, pp. 3305–3319, 2018.

[29] D. Jiang, L. Huo, and Y. Li, "Fine-granularity inference and estimations to network traffic for SDN," *PLoS One*, vol. 13, no. 5, Article ID e0194302, 2018.

Hindawi
Journal of Computer Networks and Communications
Volume 2019, Article ID 9198157, 10 pages
https://doi.org/10.1155/2019/9198157

Research Article

Proof of Concept of an IoT-Based Public Vehicle Tracking System, Using LoRa (Long Range) and Intelligent Transportation System (ITS) Services

Ricardo Salazar-Cabrera,[1] **Álvaro Pachón de la Cruz**,[2] **and Juan Manuel Madrid Molina**[2]

[1]*Telematics Department, Universidad del Cauca, Popayán, Colombia*
[2]*ICT Department, Universidad ICESI, Cali, Colombia*

Correspondence should be addressed to Ricardo Salazar-Cabrera; ricardosalazarc@unicauca.edu.co

Received 29 June 2019; Revised 1 October 2019; Accepted 30 October 2019; Published 1 December 2019

Guest Editor: Huan Zhou

Systems trying to solve mobility issues in cities, such as high levels of accidents and traffic congestion, have been developed worldwide. Intelligent Transportation Systems (ITS) services focused on urban public transport are an option contributing to solve such issues. A few intermediate cities in the Latin American context have developed some of these ITS services, which are mainly based on a tracking system for public transport vehicles. Such tracking systems have great limitations in terms of coverage, availability, and operational cost. In addition, they are commonly isolated mobility solutions, which cannot be easily integrated with other mobility services in the city because they are not based on an ITS architecture. In order to improve public transportation systems in intermediate cities, we proposed the development of an IoT-based public vehicle tracking system, using LoRa (Long Range) and ITS services. In this research, we developed the proposed system as a proof of concept. We designed and executed some experiments, in order to adjust parameters of the LoRa technology and to test its operation. This article presents the methods we followed for developing the proof-of-concept model, a description of the experiments, and their results. The results lead to conclude that the LoRa technology and an IoT-based system are adequate for implementation of a mobility service such as the one we propose, once important technical restrictions related mainly to Line of Sight (LoS) are considered. Key aspects for implementation were also identified for deploying the service (as a prototype) in the city of *Popayán*.

1. Introduction

Traffic accidents are one of the leading causes of deaths worldwide [1]. Colombia has a high percentage of deaths (between 27 and 28%), due to traffic accidents in recent years [2]. This problem is serious in intermediate Colombian cities (e.g., *Neiva, Pereira,* and *Popayán*), accounting for 36% of deaths. In addition, cities in the Latin American context have remarkable issues with regard to traffic congestion. This is evidenced in indicators such as the TomTom Traffic Index [3].

In Colombia, 25% of passengers suffering injuries in traffic accidents are passengers of public transport vehicles [4]. Such data are quite worrisome if we consider the proportion of public vehicles in Colombia. Similar situations have been identified in other Latin American countries such as Perú, Chile, México, and Ecuador [5–8]. The most common public transport vehicles in intermediate cities in Colombia and other developing countries are buses and microbuses, with a capacity ranging from 12 to 20 passengers [9]. These vehicles share the road with all the other vehicles, increasing the risk of traffic accidents. Thus, it is important to establish improvement actions to control public transport vehicles in intermediate cities without public transit exclusive lanes. The aim is to reduce the death rates due to traffic accidents and to contribute to lessen traffic congestion in these cities.

A wide variety of ITS (Intelligent Transportation System) services seeking to improve public transport service

conditions have been deployed worldwide. The vast majority of these systems use public transport vehicle tracking systems. However, there are very few cases in which the deployed ITS services use an ITS architecture specifically defined for the city. Therefore, integration of mobility services in the city is considerably difficult. In addition, only a few recent cases use improved communication technologies because the vast majority uses technologies based on mobile telephony, which has major deficiencies in coverage, availability, and operating cost.

Some of the most salient work identified in our literature review is presented below. In works such as those by Bojan et al. [10], Zambada et al. [11], Mukheja et al. [12], and Azer and Elshafee [13], ITS systems were developed to track vehicles using cellular communication technologies such as GSM and GPRS, which have great technical limitations and high operating costs. Additionally, these proposals do not use an ITS architecture as a basis. Other works such as those by Tanaka et al. [14], Boshita et al. [15], and Hattarge et al. [16] introduce the use of LoRa technology and/or its LoRaWAN (Long Range Wide Area Network) communications protocol, to track vehicles; however, such proposals were not based on an ITS architecture, they were not focused on the context of Latin American intermediate cities, and the results obtained with the use of LoRa technology were not presented in sufficient detail.

Considering the aforementioned issues, our proposal is based on an ITS architecture and technologies such as the Internet of Things (IoT) and LoRa (Long Range). Additionally, our proposal details system development, arriving at a proof-of-concept model and validating its operation through some experiments. Our research is carried out in the following four stages: design of the proposed service, development of the proof-of-concept model, execution of experiments, and analysis of results. The proposed service design is summarized because it is detailed in a previous article by the authors [17].

The development of the system focuses mainly on the components considered as critical, related to communication between vehicles and the management center and also with presentation of information to users of the system. Communication between vehicles and the management center requires sending information through gateways. Such gateways receive vehicle information using LoRa technology and transmit it to the management center using the Internet. The ideal parameters for the use of LoRa technology were not clear for the proposed mobility service, so it was necessary to develop experiments during the development of the system and then to validate its operation. Considering the context, budget limitations were also taken into account for developing the system, by using affordable hardware and free software tools. The executed experiments allowed us to determine aspects of the operation such as range of LoRa transmission, percentage of received packets, and number of messages per minute. The number of messages was determined considering the size of the message and the maximum number of vehicles that can be managed from each gateway. Finally, the analysis of results shows important restrictions that must be taken into account in the system development, mainly related to the operation with LoRa.

The remainder of the article is organized as follows: there are sections on materials and methods, executed experiments, obtained results and discussion, and conclusions and future work.

2. Materials and Methods

The research was carried out in four stages: design of the proposed service, development of a proof-of-concept model, execution of experiments, and analysis of results. The four stages are presented below in detail.

2.1. Design of the Proposed Service. A previous work of the authors features the design of an IoT-based public vehicle tracking system, using LoRa technology and ITS architecture [17]. This design was made in the five steps presented below.

In the first step, we defined a suitable ITS architecture for intermediate cities in the Latin American context. The ITS architecture deemed as adequate was based on the American ITS architecture known as ARC-IT [18].

In the second step, we created the *detailed service diagram*, using the defined ITS architecture and the service description diagrams used by ARC-IT, for services PT01 and PT08 (PT01 is Transit Vehicle Tracking and PT08 is Transit Traveler Information in ARC-IT). The detailed service diagram is presented in Figure 1. This figure shows the physical objects involved in service provision, the actors (traveler and system operator), and the information messages exchanged between actors and objects, and between physical objects.

In the third step, we selected the appropriate communication technology to link the Transit Management Center and the OBE (On-Board Equipment) on the transit vehicles, which was considered critical. Communication between the gateways and the cloud (where the Transit Management Center would be) uses the Internet. We evaluated LPWA (Low Power WAN) technologies such as LoRa, Sigfox, NB-IoT (Narrow Band IoT), and V2X technologies (Vehicle to Everything) technologies such as DSRC (Dedicated Short Range Communication) and C-V2X (Cellular V2X). After a technical analysis involving several parameters, we deemed LoRa as an appropriate technology for the PTVTS.

In the fourth step, we created the *network diagram*, which features the remaining technological components of the system. The network diagram is presented in Figure 2. The device (OBEs and Traveler Support Equipment), communication (LoRa, WiFi, and Internet), and application (web apps and software in the cloud Center subsystem) layers are clearly identified in the diagram. These layers are commonly used in IoT service architectures, which makes the designed service an "IoT-based ITS." We determined that intermediate stations with a LoRa gateway are required on the streets the vehicles use; such gateways could be located at some bus stops. These intermediate stations are necessary to collect the Transit Vehicle OBE's information.

Finally, in the fifth step, we performed an analysis of the service required characteristics for the city of *Popayán* (Colombian intermediate city), by defining the number of required intermediate stations, the number of components,

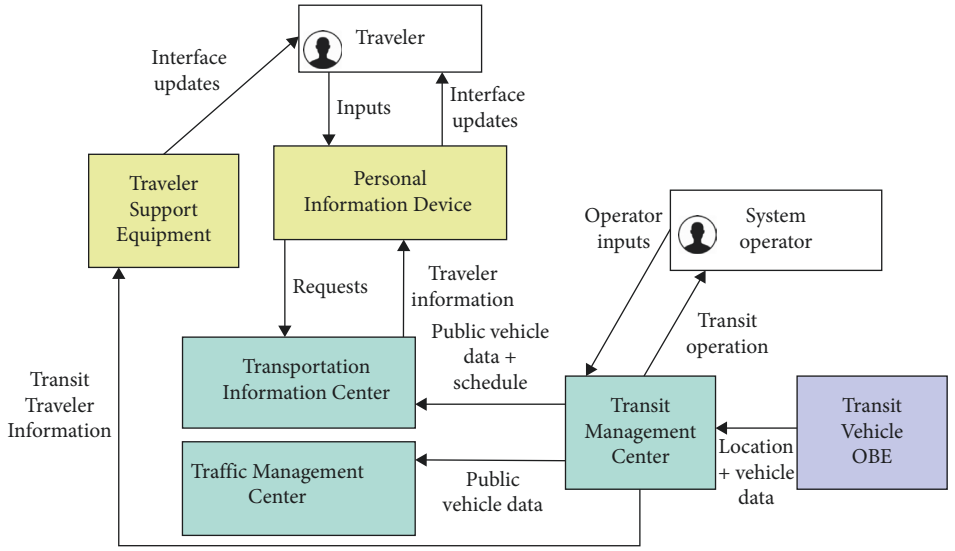

Figure 1: Detailed service diagram of public transport vehicle tracking service (PTVTS).

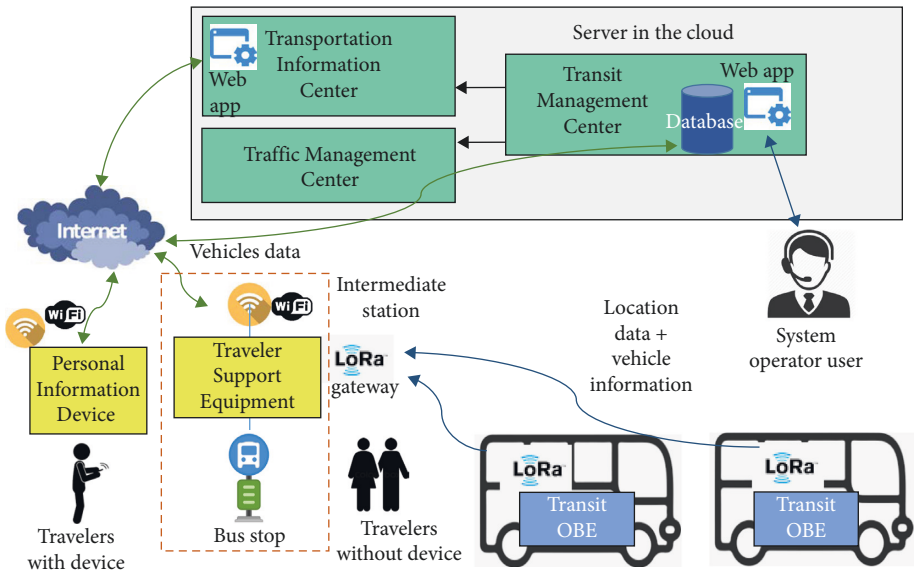

Figure 2: Network diagram of the public transport vehicle tracking service.

the recommended references for the necessary elements, an implementation budget, and an annual maintenance and support budget.

2.2. Development of a Proof-of-Concept Model. The development of the system focused mainly on the components considered as critical, for communication between the vehicles (Transit Vehicle OBE) and the server in the cloud (the *Transit Management Center* component), passing through the LoRa gateway equipment. Priority was given to these components because they are responsible for obtaining the field information and sending it to the server in the cloud. The *Personal Information Device* component was included in the development, mainly to show users system information through an appropriate interface, such as a web page. Figure 3 presents the network diagram for the proof-of-concept model.

The additional components of the designed service (Transportation Information Center, Traffic Management Center, and Traveler Support Equipment) were not developed for this version of the system because it was advisable to first assess the results obtained with the critical components, to evaluate the viability of our proposal.

For the development of the system, we first purchased the elements in the OBE and in the bus stops. Due to project budget restrictions, only two microcontroller cards and a gateway device were purchased. The selected microcontroller card was the HiLetgo ESP32 LoRa 0.96 inch OLED display, manufactured by Heltec (see Figure 4). The selected GPS was the Ublox Neo 6M. Regarding the gateway, we had the opportunity to review two references, the

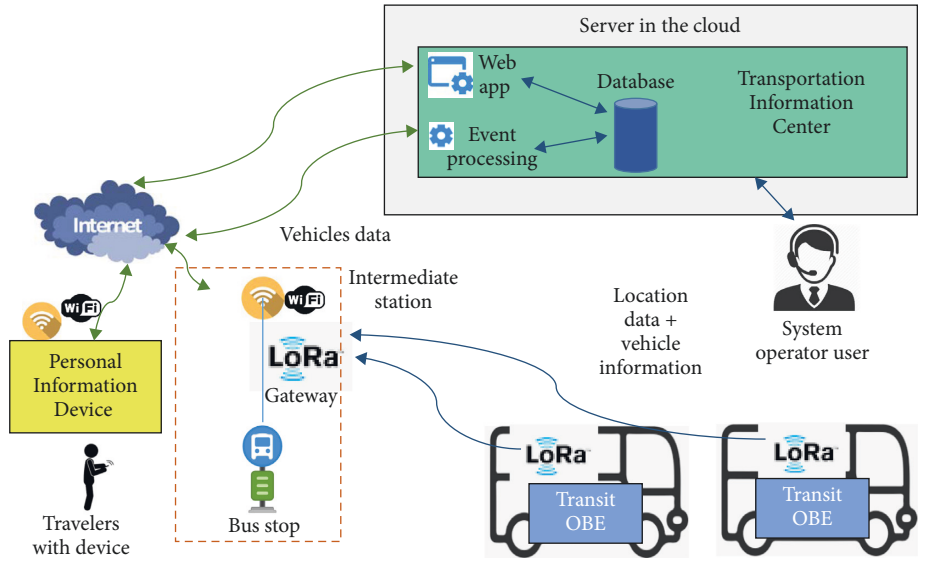

Figure 3: Network diagram of the proof-of-concept model.

Figure 4: Selected microcontroller card, HiLetgo ESP32 LoRa 0.96 inch OLED display (Heltec).

Figure 5: Selected LoRa gateway, Dragino LG01.

RAKWireless RAK831LoRa/LoRaWAN and the Dragino gateway LG01. After performing some tests with the two gateways, we deemed the Dragino gateway LG01 as the best option (see Figure 5) because this reference did not require an additional card (such as a Raspberry Pi) to operate. In addition, the Dragino gateway was easily programmable through the Arduino IDE, which was not possible with the other gateway.

Once we selected and acquired the elements, we carried out some experiments prior to final development (see the *Executed Experiments* section). Finally, we developed the software required to send the information collected by the microcontroller card (main OBE component of each vehicle) to the gateway, through LoRa messages. The information for this case was vehicle location (latitude and longitude), speed, and altitude, taken from the GPS device. We also developed the software for receiving the LoRa messages sent by the OBEs and transmitting the information through the Internet to the server in the cloud. Both modules were developed using the Arduino IDE (Integrated Development Environment) tool. The source code for the modules is available online (see the *Data Availability* section).

In order to send the information from the OBE devices to the gateway, we evaluated the possibilities (through testing) of establishing a LoRaWAN or simply sending LoRa messages. The LoRaWAN specification is a Low Power, Wide Area (LPWA) networking protocol designed to wirelessly connect battery operated "things" to the Internet in regional, national, or global networks [19]. LoRaWAN architecture is deployed in a star-of-stars topology, in which gateways relay messages between end devices and a central network server. The gateways are connected to the network server via standard IP connections and act as a transparent bridge, simply converting RF packets to IP packets, and vice versa [19]. We used the TTN platform (The Things Network) to perform tests with LoRaWAN. The Things Network (TTN) enables low-power devices to use long-range gateways to connect to an open-source, decentralized network to exchange data with applications. The connection of devices to TTN could be made by OTAA (over-the-air activation) mode or ABP (activation by personalization) mode. OTAA is the preferred and most secure way to connect with TTN [20]. In OTAA, when devices join the network, a dynamic

DevAddr (Device Address) is assigned and encryption keys are negotiated with the device. ABP mode is used when it is required to encrypt the DevAddr and device encryption keys [20]. We used LoRaWAN in OTAA mode, but the connection time of the devices was too long, compared to the sending time of LoRa messages without the LoRaWAN protocol. This might be due to some particularity of the LoRaWAN protocol, or the processing done in the test. We reviewed literature in this regard [21–23] trying to find a solution and ran some tests related to data rate and access channels (detailed in experiment 2). Finally, we achieved connection to the LoRaWAN in an acceptable time of a few seconds; however, connection through LoRa messages proved to be faster. Thus, considering vehicles connect to several gateways along their route, we decided to send LoRa messages as the best option, without establishing a LoRaWAN.

The sending and receiving of LoRa messages require some special parameters to be determined, such as the frequency, the Spread Factor (SF), and the bandwidth (BW). Regarding the frequency, we worked in the 902–928 MHz range, used in the United States (US), selecting 915 MHz as the channel for sending/receiving data. According to the LoRa Alliance in its Regional Parameters document v1.1. [24], this would be the frequency range allocated to Colombia for this technology. Literature reviewed [25–28] on LoRa recommends some values for SF and BW; however, we performed some tests modifying those values (experiment 2, *Executed Experiments* section), with the aim of optimizing range, message size, and frequency of sending messages. We determined that the appropriate values were 7 for the SF (which can be set between 1 and 12) and 125 KHz for the BW (which can be 125 KHz, 250 KHz, or 500 KHz). Another important parameter is the *Sync Word*, which must be the same for both sender and receiver.

In addition to the software for the OBE and the gateway, we wrote a program in the cloud server, for receiving the messages from the gateway and storing them in the *Event Processing* database (Figure 3). We used the XAMPP platform ([29]), which features a web server (Apache), a programming tool (PHP), a database engine (MariaDB), and a database administrator (phpMyAdmin). We used RESTful actions for communication between the LoRa gateway and the *Transit Management Center* in the cloud. These actions use the POST HTTP method in the LoRa gateway software to send information of all vehicles and the GET HTTP method in the cloud server program to capture the data and record it in the database. A link to the source code for this program is also included in the *Data Availability* section of this article.

Finally, we developed a web application using XAMPP, for the two types of users identified for the system (operator and traveler), so that they could visualize the location of the public transportation vehicles on a map. Figure 6 shows the user login interface. Figure 7 shows the operator user interface, for querying the location of any vehicle at any time and date of the day. Results are presented in a table and also on a map, using Google APIs. The end user can also see the latest location of a vehicle, but the query is limited to current date/time and to a certain number of last locations.

Figure 6: Login interface for the system user.

2.3. Executed Experiments. We executed three experiments to test the operation of the components and their integration. Two additional experiments were also designed and executed to evaluate system operation.

The first experiment, carried out during the development of the system, was to establish a point-to-point connection between the two microcontroller cards for sending a test LoRa message. One of the cards was programmed as sender and the other as receiver. Several test messages were sent every 3 seconds from the card configured as sender, expecting to receive all the messages on the card configured as receiver without any problems. To view the messages sent and received, we used the *Serial Monitor* in the Arduino IDE. Figure 8 presents the architecture for experiment 1.

In the second experiment, we used the same configuration of the initial experiment, but the card acting as a LoRa receiver was also configured as a WiFi connection client (using the WiFi internal module in the ESP32 card) in order to relay the received information to a web server located on a computer in the same WiFi network (using XAMPP and a program named *Event Processing*). The *Event Processing* module received the messages and stored them in a local database. In this experiment, we aimed at determining the appropriate SF and BW parameters, by varying them and verifying in which cases a signal with greater power was obtained in the receiver, using the parameter received signal strength indicator (RSSI), measured in dBm. Several test messages were also sent every 3 seconds from the card configured as sender. We used the *Serial Monitor* tool of the Arduino IDE to visualize sent and received messages. We used XAMPP's phpMyAdmin tool to visualize the data recorded in the database. Figure 9 presents an architecture for experiment 2.

In the third experiment, the Dragino gateway was configured to receive the test LoRa messages from the two microcontroller cards, both configured as sender only. The Dragino gateway was also configured to send the information to the web server used in the previous experiment. In this experiment, tests were carried out to determine an adequate message size, to be able to send them with a few seconds of

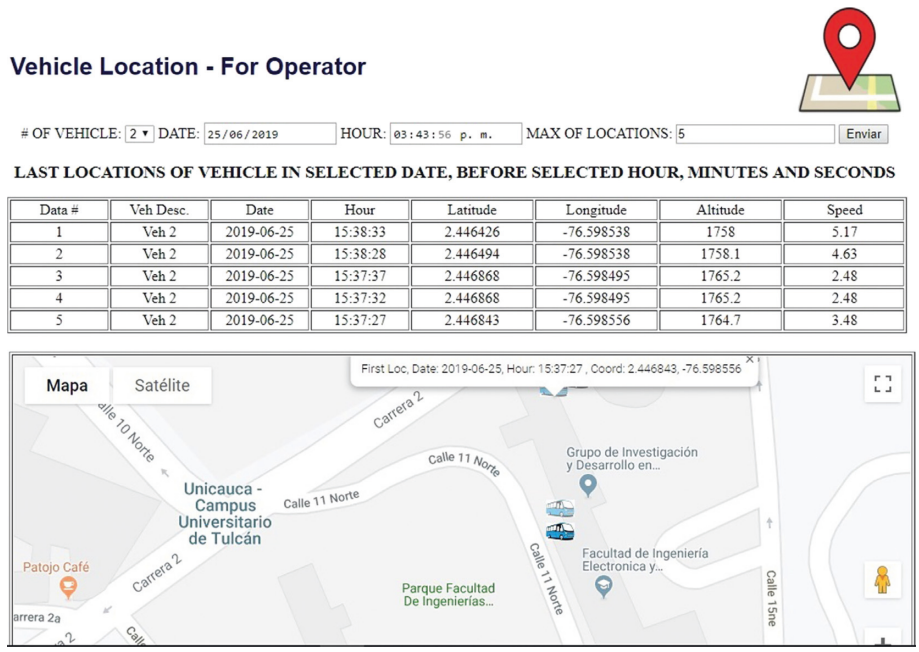

Figure 7: Public vehicle tracking interface for the system operator.

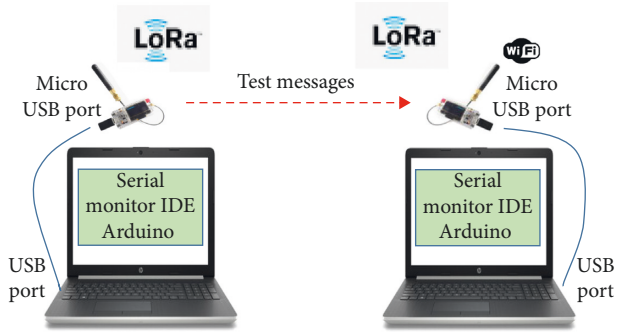

Figure 8: Experiment 1 architecture.

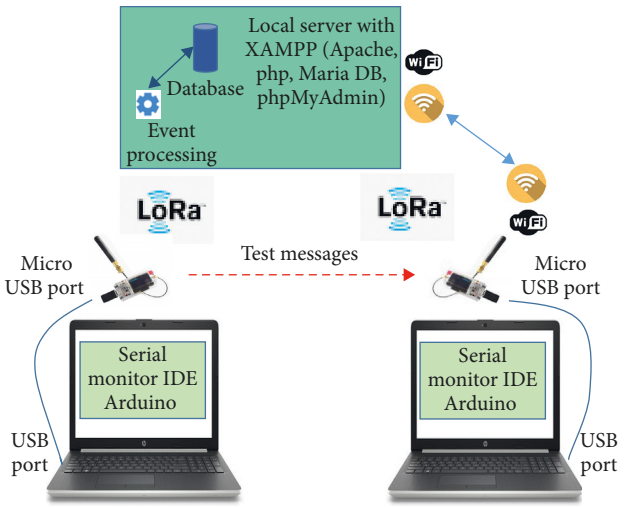

Figure 9: Experiment 2 architecture.

difference and to receive messages from the two cards at the gateway. This is due to the fact that mobility services related to tracking require sending messages with a high frequency (for example, 10 times per minute), so that the location can be determined in real time or as close as possible.

In this experiment (third), we performed tests with LoRaWAN in the OTAA mode, showing that the devices took much time registering on the network. The cause for this long connection delay was researched [21–23]. We found out that a LoRaWAN operates in several frequency channels that are determined by the gateway configuration. The number of allocated channels depends on regional restrictions and the network options [21]. We also found out that the data rate parameter defined by the SF and the bandwidth is relevant to the LoRaWAN configuration. Some tests related to these mentioned aspects (access channels and data rate) were performed, initially modifying the access channels and maintaining the data rate, and subsequently improving at this point and identifying the ideal channels, the data rate was modified, identifying the best channel, which allowed to reduce the connection time of the devices to the network to a few seconds. However, the connection time through LoRa messages, without the establishment of a LoRaWAN, remained faster and more efficient. In addition, the type of service to be implemented requires that the devices (located in the vehicles) connect to several gateways along their route, so we consider sending LoRa messages as ideal, without using the LoRaWAN configuration. Figure 10 presents the architecture for experiment 3.

The fourth experiment was executed with the system already developed. The microcontroller cards were programmed with the latest version of our software, which includes the correct GPS configuration, the appropriate size of the message, the LoRa parameters (SF, BW, and Sync Word). The software was configured to only send information without receive acknowledge, in order to be able to send messages more frequently. The Dragino gateway software was also configured with the latest version of our software, including LoRa parameters, Internet connection

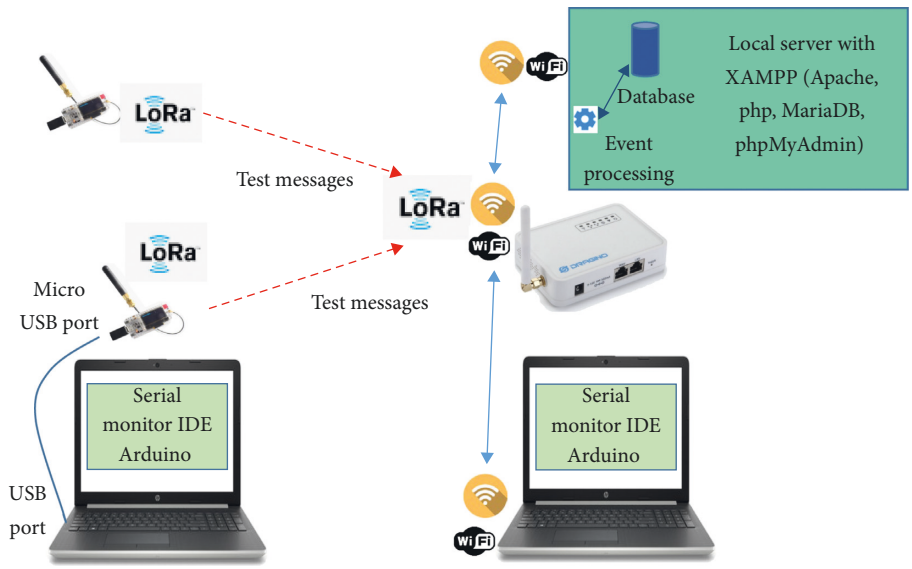

Figure 10: Experiment 3 architecture.

via WiFi, and sending data to a server in the cloud. The gateway was located on the terrace of a 4-floor building of the University of Cauca, and the OBE devices were located in the University Sports Center, which is in front of the aforementioned building, at approximately 400 meters. Information collected by each one of the microcontroller cards was sent every 5 seconds approximately; we expected to receive all sent messages in the Dragino gateway. Figure 11 presents the architecture for experiment 4.

Finally, in the fifth and last experiment, we used the same setup of the fourth experiment, but the two OBE devices were located in vehicles, and each vehicle did a different route through the streets near the building where the gateway was located. The route for each vehicle was approximately 2 km. The size of the messages and the sending frequency was the same as in the previous experiment. Experiment 5 architecture is similar to Figure 11, but the OBE devices were located in vehicles.

3. Results and Discussion

We present the results obtained in the three experiments performed during system deployment and two experiments performed with the already deployed system.

In the first experiment, the communication of the two LoRa modules (end devices) was tested at varying distances (from 3 to 200 meters), with the first module acting as sender and the other as receiver. We verified the correct sending and reception of data.

The results for the first experiment were successful. 100% of the sent packets were received, even with some minor obstacles (walls and windows) in the LoS. When the number of obstacles in the LoS increases, messages were not received. We increased the frequency of sending messages to determine if this affected their correct reception; however, packets were not lost even sending a message every 3 seconds, a rate much higher than the required rate for the deployed service.

In the second experiment, we tested the two LoRa modules with the same configuration of experiment 1. In addition, the receiver LoRa module was also configured as a gateway to send the data to a local server.

The results for the second experiment were successful too. 100% of the messages sent were received, as long as there were no significant obstacles in the LoS. We performed tests with distances up to 400 meters, sending messages once every 3 seconds. During this experiment, we measured the RSSI parameter, to determine the signal levels in the receiver by varying distances between modules and adding obstacles. When we only varied the distance, differences in RSSI levels of the messages were not considerable. When we increased the number of obstacles and the distance, the RSSI levels decreased considerably in the cases where the message was received; in some cases (with a high number of obstacles), the messages were not received. Additionally, in this experiment, maintaining a fixed distance and varying the number of obstacles, we modified the SF and BW parameters to determine which combination would yield a better RSSI. We determined that ideal values were 7 for SF and 125 KHz for BW.

In the third experiment, we tested the two LoRa modules acting as sender and the Dragino device acting as receiver and gateway. During the sending of data in the third experiment, we identified that although LoS existed between the end device and the gateway, some of the sent packets were not received or were received with unexpected characters in the middle of the data. When this happened, the Dragino gateway stopped receiving data (specifically from the device from which the wrong data were received) for a few seconds, and then the gateway resumed receiving data normally from the two devices. In the tests carried out, approximately 2% of the packets sent from each of the cards acting as senders were not received. We determined that reception problems are due to interference between the two signals that arrive at the gateway; however, taking into

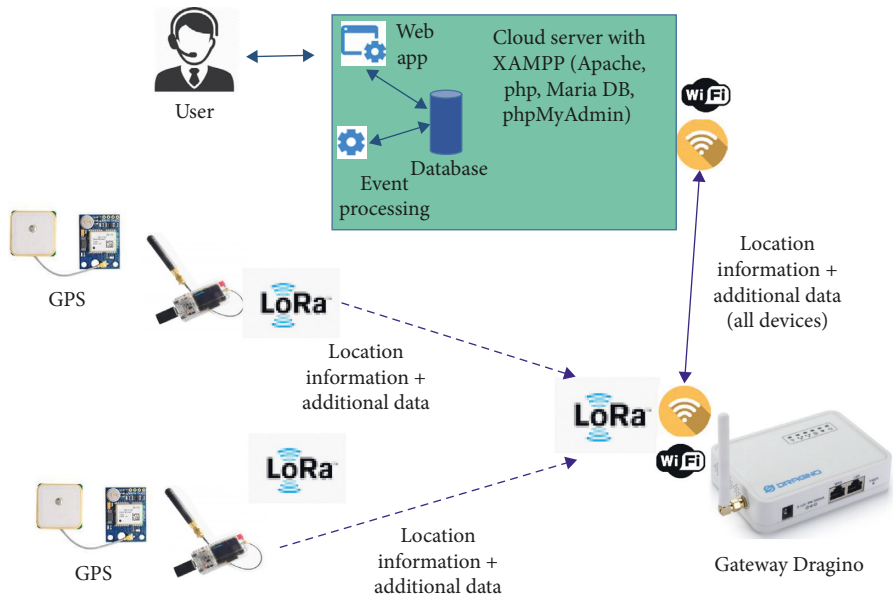

Figure 11: Experiment 4 architecture.

account the frequency with which the packets are sent (1 time every 3 seconds), this problem does not represent a major inconvenience for tracking public transport vehicles in real time. However, it is recommended for future work, to perform some tests with a greater number of end devices, to verify if the percentage of not received packets is increased or maintained. If that 2% is maintained or does not increase too much, detected interference would be manageable.

In the fourth experiment, the components were configured in a similar way to the third experiment, but using real GPS-generated data, and a cloud server for data collection. Experiment 4 showed some packet loss from each of the end devices, approximately 2%, similar to the results of experiment 3. Although we tried to decrease the packet sending frequency, packet loss was not affected. To avoid inserting erroneous data in the database, when the packet arrived with unexpected characters, we made a validation in the *event processing* program that allowed us to identify format errors. Packets with errors were not recorded in the database. In this experiment, we did not find LoS problems.

Finally, in the fifth experiment, the configuration of components was the same as the previous experiment, but with moving end devices. Initially, the experiment was not successful; a large percentage (greater than 60%) of the sent messages was not received. The cause that was initially considered the most likely was the large number of obstacles in the LoS. Although the Dragino gateway was located in the roof of a tall building (approximately 25 meters), it was not possible to obtain LoS with most sections of the routes, and the obstacles were considerable (mainly, other buildings). To improve the percentage of received messages, we researched some other possible causes and solutions [21–23]. We found out that the main cause of the high percentage of lost packets was actually due to a large number of obstacles in the LoS and the Spread Factor used because the value of 7 has a low range. According to [22], increasing the SF parameter (to a value between 8 and 12) also increases the range that can be achieved but decreases the data rate and increases the ToA (Time on Air, elapsed time since the packet is sent until it reaches its destination). In our experiment, and in general for public vehicle tracking, a high data rate is not required, while a good signal range is preferred.

One possible way to modify the relevant LoRa parameters is through an adaptive data rate (ADR) algorithm [23], which features an automatic learning method using the different transmission parameters. However, considering the low number of devices in our experiment and the low number of parameters to modify, we consider this approach is not necessary in our case.

Considering our findings, we reran experiment 5 and measured the new results. We decided to manually modify the SF parameter from 8 to 12, making measurements of the lost packets for each of the values, keeping the BW parameter fixed at 125 KHz. When performing tests with SF values greater than 7 until reaching a value of 12, the best results were obtained with an SF of 10, achieving a decrease in the percentage of lost packets from 60% to 28%, with a final data rate of 10 messages per minute. Additionally, it is important to mention that the largest number of lost packets was presented at sites with a large number of obstacles in the LoS.

The most salient results of our experiments are as follows:

(i) LoS between the gateway and the end devices in our system was very relevant, due to the fact that the number of possible obstacles to establish communication was relatively low.

(ii) The change in the size of the message (between 10 and 35 characters) was not relevant to improve the communication conditions, considering that we only had two devices communicating with a gateway, sending one message at least every three seconds. However, according to the reviewed literature, when the number of devices that communicate with

the gateway is high, having a certain message size could affect the maximum possible message frequency.

(iii) The *Bandwidth* and *Spread Factor* parameters recommended for the frequency range used in the US (902–928 MHz, same for Colombia) are 125 KHz for bandwidth and a Spread Factor of 7. However, we verified that if a high data rate is not required, it is possible to use Spread Factors greater than 7 (between 8 and 12), to reduce the number of lost packets.

(iv) When we tested two devices sending LoRa messages to the gateway, approximately 2% of the total packets sent were lost. We consider that such packet loss may be due to interference between the two signals; however, because the frequency of sending messages is relatively high, this loss would not be significant to track public vehicles.

(v) Although the number of lost packets in the final experiment (where moving vehicles were used) is relatively high (28%), we found that lost packets occurred mainly in sectors where there were too many obstacles in the LoS. This calls for the importance of locating the gateways in places tall enough to avoid as many obstacles in the LoS as possible.

4. Conclusions and Future Work

The proposed tracking system for public transport vehicles through an IoT-based system, LoRa technology, and ITS services is suitable for implementation in an intermediate city, if some important technical aspects of LoRa operation are considered. These technical aspects were identified in the experiments carried out in this work.

The most relevant technical aspects of LoRa operation to be taken into account are an adequate LoS between the gateway and the devices in the vehicles, which requires a strategic location of the gateways in places with sufficient height and visibility to the roads from which the vehicles will send the messages (number of obstacles between the gateway and the roads should be as small as possible); the Spread Factor (SF) should be adjusted between 8 and 12 for each one of the gateways, and tests for packet loss should be performed in the area where the messages are expected to be received. In case it is not possible to carry out the tests, an SF of 10 is recommended, according to the tests performed in our work; for the recommended SF to be a good option, data rate should not be too high because the ToA is increased.

With regard to the technical characteristics of the developed system, it was possible to send messages with location data (latitude and longitude) and speed of vehicles with LoRa technology, with an adequate message size, an acceptable range, a sufficient sending frequency for the type of service, and a manageable packet loss. However, this was achieved in cases where LoS had no obstacles or the number of obstacles was low. Although in the final experiment, approximately a quarter of the messages sent by the devices were not received, in a type of tracking system where the device located in the vehicle sends information with a sufficiently high frequency (approx. 10 times per minute), such losses are acceptable. In addition, a better location of gateway devices improves LoS and would reduce packet losses considerably.

In our prior research, we had estimated a total number of 15 gateways for covering the city of *Popayán*, which according to the results obtained from the range and LoS experiments is a low number. In addition to the factors that were taken into account in the service design proposal, such as the city dimensions and road location, it is very important to determine strategic tall sites where gateways can be located. In most cases, these gateways will not be able to be located at the bus stops (as estimated in the preliminary design) because range would be very limited.

As a future work, in addition to the strategic location of the system gateways, in order to achieve the widest possible range in communication and avoid higher deployment costs, other relevant parameters could be adjusted in the LoRa communication, e.g., using a larger range antenna in the gateway, or the use of a different brand/model of gateway. Also, for the future, it is very important to test the operation of the system with a greater number of end devices, to determine if this considerably increases packet loss beyond 2% of the total.

Data Availability

The programs data (developed programs for the end devices, the Dragino gateway, and the Event Processing component) used to support the findings of this study are available from the corresponding author upon request.

Conflicts of Interest

The authors declare that there are no conflicts of interest regarding the publication of this paper.

Acknowledgments

This research was funded by Universidad ICESI and Universidad del Cauca. Publication of this article was funded by Universidad ICESI, School of Engineering.

References

[1] World Health Organization, "Report on the world situation of road safety 2015," 2019, http://www.who.int/violence_injury_prevention/road_safety_status/.

[2] National Institute of Legal Medicine and Forensic Sciences, Centro de referencia nacional sobre violencia 2018, 2019, http://www.medicinalegal.gov.co/documents/20143/217010/Boletin+mensual+junio-2018.pdf/57a48178-ba32-2725-caf2-27b9f2079114.

[3] Tom Tom Traffic Index. 2019 https://www.tomtom.com/en_gb/traffic-index/.

[4] D. Vargas, *Comportamiento de Muertes y Lesiones en los Accidentes de Tránsito, Colombia*, National Institute of Legal Medicine and Forensic Sciences, Bogota, Colombia, 2015, http://www.medicinalegal.gov.co/documents/20143/49523/Accidentes+de+transporte+primera+parte.pdf.

[5] INEI (National Institute of Statistics and Informatics of Perú), "Análisis de los accidentes de tránsito ocurridos en el 2014," 2014, https://www.inei.gob.pe/media/MenuRecursivo/publicaciones_digitales/Est/Lib1308/cap03.pdf.

[6] SCT (Secretary of Communications and Transportation, Mexico), "Estadística de accidentes de tránsito," 2017, http://www.sct.gob.mx/fileadmin/DireccionesGrales/DGST/Estadistica_de_accidentes/A%C3%B1o_2017/RESUMEN_2017.pdf.

[7] CONASET (National Traffic Safety Commission), "Estadísticas generales de accidentes de tránsito, Chile," 2017, https://www.conaset.cl/programa/observatorio-datos-estadistica/biblioteca-observatorio/estadisticas-generales/.

[8] National Institute of Statistics and Census, "Anuario de transporte 2016, ecuador en cifra," 2016, http://www.ecuadorencifras.gob.ec/documentos/web-inec/Estadisticas_Economicas/Estadistica%20de%20Transporte/2016/2016_AnuarioTransportes_%20Principales%20Resultados.pdf.

[9] S. Valbuena, *Muertes y Lesiones No Fatales en Accidentes de Tránsito, Colombia*, National Institute of Legal Medicine and Forensic Sciences, Bogota, Colombia, 2011, http://www.medicinalegal.gov.co/documents/20143/49511/Accidentes+De+Transito.pdf.

[10] T. M. Bojan, U. R. Kumar, and V. M. Bojan, "An internet of things based intelligent transportation system," in *Proceedings of the 2014 IEEE International Conference on Vehicular Electronics and Safety*, pp. 174–179, IEEE, Hyderabad, India, December 2014.

[11] J. Zambada, R. Quintero, R. Isijara et al., "An IoT based scholar bus monitoring system," in *Proceedings of the 2015 IEEE First International Smart Cities Conference (ISC2)*, pp. 1–6, IEEE, Guadalajara, Mexico, October 2015.

[12] P. Mukheja, M. K. Kiran, N. R. Velaga, and R. B. Sharmila, "Smartphone-based crowdsourcing for position estimation of public transport vehicles," *IET Intelligent Transport Systems*, vol. 11, no. 9, pp. 588–595, 2017.

[13] M. A. Azer and A. Elshafee, "A real-time social network-based traffic monitoring & vehicle tracking system," in *Proceedings of the 2018 13th International Conference on Computer Engineering and Systems (ICCES)*, pp. 163–168, IEEE, Cairo, Egypt, December 2018.

[14] M. S. Tanaka, Y. Miyanishi, M. Toyota et al., "A study of bus location system using LoRa: bus location system for community bus "Notty"," in *Proceedings of the 2017 IEEE 6th Global Conference on Consumer Electronics (GCCE)*, pp. 1–4, Nagoya, Japan, October 2017.

[15] T. Boshita, H. Suzuki, and Y. Matsumoto, "IoT-based bus location system using LoRaWAN," in *Proceedings of the 2018 21st International Conference on Intelligent Transportation Systems (ITSC)*, pp. 933–938, IEEE, Maui, HI, USA, November 2018.

[16] S. Hattarge, A. Kekre, and A. Kothari, "LoRaWAN based GPS tracking of city-buses for smart public transport system," in *Proceedings of the 2018 First International Conference on Secure Cyber Computing and Communication (ICSCCC)*, pp. 265–269, IEEE, Jalandhar, India, December 2018.

[17] R. Salazar-Cabrera, Á. P. de La Cruz, and J. M. Madrid Molina, "Fleet management and control system from intelligent transportation systems perspective," in *Proceedings of the 2019 2nd Latin American Conference on Intelligent Transportation Systems (ITS LATAM)*, pp. 1–7, IEEE, Bogota, Colombia, 2019.

[18] ARC-IT, "National ITS architecture," 2018, http://local.iteris.com/arc-it/.

[19] LoRa Alliance, "What is the LoRaWAN® specification?," 2019, https://lora-alliance.org/about-lorawan.

[20] The Things Network (TTN), "LoRaWAN network server," 2019, https://www.thethingsnetwork.org/docs/network/.

[21] D. Bankov, E. Khorov, and A. Lyakhov, "On the limits of LoRaWAN channel access," in *Proceedings of the 2016 International Conference on Engineering and Telecommunication (EnT)*, pp. 10–14, Moscow, Russia, November 2016.

[22] R. Sanchez-Iborra, J. Sanchez-Gomez, J. Ballesta-Viñas et al., "Performance evaluation of LoRa considering scenario conditions," *Sensors*, vol. 18, p. 772, 2018.

[23] N. Benkahla, H. Tounsi, Y. Song, and M. Frikha, "Enhanced ADR for LoRaWAN networks with mobility," in *Proceedings of the 2019 15th International Wireless Communications & Mobile Computing Conference (IWCMC)*, pp. 1–6, Tangier, Morocco, 2019.

[24] LoRa Alliance, "Regional parameters," 2017, https://lora-alliance.org/sites/default/files/2018-04/lorawantm_regional_parameters_v1.1rb_-_final.pdf.

[25] R. El Chall, S. Lahoud, and M. El Helou, "LoRaWAN network: LoRaWAN network: radio propagation models and performance evaluation in various environments in Lebanon," *IEEE Internet of Things Journal*, vol. 6, no. 2, pp. 2366–2378, 2019.

[26] A. M. Yousuf, E. M. Rochester, B. Ousat et al., "Throughput, coverage and scalability of LoRa LPWAN for internet of things," in *Proceedings of the 2018 IEEE/ACM 26th International Symposium on Quality of Service, IWQoS 2018*, June 2018.

[27] F. Adelantado, X. Vilajosana, P. Tuset-Peiro, B. Martinez, J. Melia-Segui, and T. Watteyne, "Understanding the limits of LoRaWAN," *IEEE Communications Magazine*, vol. 55, no. 9, pp. 34–40, 2017.

[28] M. Cattani, C. A. Boano, and K. Römer, "An experimental evaluation of the reliability of LoRa long-range low-power wireless communication," *Journal of Sensor and Actuator Networks*, vol. 6, no. 2, p. 7, 2017.

[29] XAMPP, Apache Friends, https://www.apachefriends.org/es/index.html.

Hindawi
Journal of Computer Networks and Communications
Volume 2019, Article ID 3217369, 16 pages
https://doi.org/10.1155/2019/3217369

Research Article

Energy-Efficient Coalition Games with Incentives in Machine-to-Machine Communications

Raymond W. Juma, Anish M. Kurien, and Thomas O. Olwal

Department of Electrical and Electronic Engineering, Tshwane University of Technology, Pretoria, South Africa

Correspondence should be addressed to Raymond W. Juma; rjwekesa@gmail.com

Received 14 February 2019; Revised 13 May 2019; Accepted 23 May 2019; Published 16 June 2019

Guest Editor: Huan Zhou

The need to achieve energy efficiency in machine-to-machine (M2M) communications has been a driver of the use of coalition game-based cooperative communication schemes. The proposed schemes have shown good energy-efficient performance results in the recent past. However, sustaining cooperation amongst coalition games of M2M devices from different network-operating authorities requires appropriate incentives. A review of the literature demonstrates that a limited number of contributions have considered the use of coalition games with incentives in M2M communications. In this paper, an energy-efficient coalition game with incentives in M2M communications is proposed. This work considers a Sierpinski triangle technique to partition M2M devices into multiple networks of hierarchical zones. Based on the constructed zones, a contract-modelled incentive is invoked to stimulate multihop transmissions between devices up to the BS/sink. The results obtained demonstrate that the proposed approach is on average 10% more energy efficient than the closely related existing algorithm, the coalition game theoretical clustering (CGTC).

1. Introduction

The introduction of M2M communications has catapulted the automation of various tasks in real time. The applications of M2M have been embraced today in the sectors of transport, military, healthcare, and smart cities. However, despite the growing interest of M2M technologies, one of the greatest challenges faced by M2M devices is the limited battery lifetime of operations. There is thus a need to prolong the operation of M2M devices while ensuring a stable quality of service/quality of experience (QoS/QoE). This can be achieved through cooperation among the devices in the network. Zhou et al. [1] utilise the data offloading technique through vehicular ad hoc networks (VANETs). Huang et al. [2] describe the use of credit-based clustering (CBC) scheme to encourage sharing among devices in the same social network. The application of cooperative schemes in energy-efficient management has been proposed by Raymond et al. [3] and Olwal et al. [4]. Cooperative schemes that invoke game theory are examined for energy efficiency in WSNs [5]. Over years, the application of game theory has had a considerable impact on a sizeable number of disciplines that include engineering, economics, political science, philosophy, and even psychology [6].

In recent years, game theory has been applied in the analysis of communication networks. In an effort to minimise energy consumption in a network, an efficient-energy consumption protocol (EECP) utilises fixed clusters and applies the random weight technique in selection of cluster heads (CHs) [7]. The concept of game theory is applied during multihop data transmission to the sink. A cooperative game algorithm for routing purposes which considers rewarding cooperative devices and punishing noncooperative devices is proposed for energy management in WSNs [8].

A coalition game takes into consideration the benefits of all the players in the network; players adopt strategies that strengthen the utility of another player. It may be considered an appropriate approach when considering its application in the implementation of fair and well-

organised cooperative strategies in communication networks [9]. Through games of coalitions, it has been argued by Bacci et al. [10] that huge computation overheads that are associated with larger networks may be avoided. AlSkaif et al. [11] argue that coalitional games are characterised by group formation that demonstrates better performance in energy efficiency when compared to noncooperative games A further benefit of coalition game theory (CGT) is demonstrated through the reduction of power consumption in a WSN that is achieved as a result of the formation of coalition structures [12]. Under these structures, players choose strategies to maximise their own utility as a group. Such group-based strategies enable individuals to consume less energy and operate for a longer period than when each player could have strategized independently. Earlier studies had explained that a selfish node or device in a communication network caused network performance degradation [13, 14]. Due to the distance effect, the devices that were located farther from each other would consume more energy before reaching the processing device/sink.

The need to achieve energy efficiency in M2M communications has been attained through the use of coalition game-based cooperative communication schemes [5, 7, 15]. However, sustaining cooperation amongst coalition games of M2M devices from different network-operating authorities or regions is a great challenge. This is due to the selfish behaviour of some of the devices or operating authorities that prefer to conserve their energy instead of consuming it to assist other devices to reach the sink/BS. To mitigate this challenge, the study proposes a coalition game theoretical clustering with incentive (CGTCI) algorithm. The novel approach proposed considers a Sierpinski triangle technique to partition distributed M2M devices into multiple networks of hierarchical zones. Based on the constructed zones, coalition structures supervised by the devices elected as cluster heads are developed in the zones located far from the BS. Devices closer to the BS are not organised into coalition structures. A contract model-based incentive is invoked to stimulate multihop transmissions up to the BS/sink. The main contributions of this work can be summarised as follows:

(i) A novel algorithm, coalition game theoretical clustering with incentive (CGTCI), is proposed to minimise energy consumption in M2M communications.

(ii) The proposed algorithm CGTCI is designed which starts with the partitioning of M2M devices into multiple networks of hierarchical zones, formation of coalition structures in the created hierarchical multiple zones, and invoking of a contract-modelled incentive to stimulate multihop transmissions up to the BS/sink.

(iii) It is demonstrated through simulations that the proposed algorithm, CGTCI, improves energy efficiency among the M2M communications when compared with the closely related traditional approaches: CGTC [15], CG-DC (an improvement of low-energy adaptive clustering hierarchy (LEACH)) [16], Raymond et al. [3], and noncoalition game (NCG) algorithms.

The remainder of this paper is organised as follows: Section 2 presents related works on coalition games. Section 3 introduces the fundamentals of the proposed algorithm. In Section 4, the system model is described. Section 5 describes the proposed solution. In Section 6, the performance and simulation results are evaluated. Section 7 finally highlights conclusions and future work.

2. Related Works

The discussions of coalition games have been extensively presented in the existing literature. This section leverages such contributions made previously to review the most related and credible studies regarding energy efficiency in communication networks. The hybrid game theory and a distributed cluster technique are applied in WSNs to control energy consumption by Yang et al. [17]. Each node has a payoff that is designed based on various parameters that include node degree and distance to the base station. Based on this approach, each node computes its equilibrium probability by applying the parameters of the game. The application of equilibrium probability by the node enables it to decide its suitability of being a cluster head (CH). The node attains a good trade-off between minimizing energy dissipation and providing the required services effectively.

Yue et al. [18] propose a coalition game model which has been derived by integrating both the Markov process and theoretical approach for energy-efficient WSNs. The performance tests of the proposed model show that the lifetime and effective reachability for low-density WSNs are increased. However, the model was not evaluated for a dense network to ascertain its effectiveness of energy efficiency.

Wu et al. [19] examine data transfer strategies that are specified in relation to the proportion of the data sent by a node and that of the data forwarded by a node for energy-efficient WSNs. The formation of coalitions is based on a Markov process. The concept of determining the absorption coefficient to measure the coalitional profiles is introduced. Nash equilibrium (NE) is used to determine the formed coalitions' approximate data transfer strategies. However, finding the exact NE in this proposal is a nondeterministic polynomial (NP) time complex problem. It is advised that a low computationally complex alternative strategy be considered.

Jing and Aida [20] present a cooperative game theoretical model for clustering algorithms in which nodes balance the energy consumption and maximise their network lifetime. The selfish behaviour of nodes in noncooperative games expedites network partition and results in an unfair residual energy distribution within the network. The work by Jing and Aida [20] considers an algorithm in which there is a trade-off in the individual cost and the network-wide cost of sensor nodes in forming a coalition. In this respect, a candidate cluster head (CCH) cooperates with a node considered to be close and almost equivalent in terms of energy (node with redundant energy), and the whose

transmission covers a long distance. The Shapley value that has anonymity, dummy property, and additivity property is introduced to assign a single cost allocation to the cost-sharing game. The Shapley value through random ordering of nodes provides a relatively anonymous solution, where agents' change of names does not alter their cost shares. However, the initial candidate selection in this approach is partly random and does not guarantee the choice of the most suitable candidate as a CH. In this approach, the direct communication between the selected device and the BS contradicts the scalability benefits achieved with the coalition game clustering.

Afsar [15] shows how a coalitional game theoretical clustering (CGTC) algorithm can be used to control energy consumption in WSNs through the adoption of multihop communications. The coalitions are demarcated into two major groups based on the location (i.e., either far or in the vicinity) of sensor nodes in relation to the BS. A set of nodes with the highest residual energy in the far region are referred to as coalition head nominees (CHNs) which initiate cooperative games within their surroundings. The CHNs along with two other nodes then shape final coalitions. The vicinity region on the contrary considers that small coalitions are formed to tackle the energy-consuming data-relaying task. In the CGTC approach, local parameters such as residual energy, number of neighbours, and proximity to the BS are important in forming the coalitions since the main objective is energy efficiency (EE). The Shapley value is applied to distribute the average of marginal contributions to coalitions generated. However, the random candidate election could easily result in the acceleration to a dead state in cases where a candidate of low residual energy is picked as a cluster head.

Miao and Xu [21] discuss a power control solution that is based on the trade-off between energy efficiency and end-to-end delay that is applied as a technique to improve energy consumption in WSNs. A cooperative coalitional game is proposed to obtain a power control solution that achieves a fair distribution of the total cost amongst sources. It was observed that the minimization of delay is achieved by minimizing the remaining energy level. Each source node seeks to minimise its utility function of the discounted sum of transmission power increased cost and the source-to-sink delay cost. The Shapley value is used as a solution of the cooperative allocation game for fairness dissemination of the gains achieved as evaluated by Yeung and Petrosjan [22].

Tan et al. [23] develop a bidirectional cooperative clustering model that applies a cost-sharing game for EE. The algorithm examines the cooperation of cluster members and cluster heads (CHs) for reducing energy consumption in the network. The authors highlight that an algorithm based on game theory can be applied in the CH selection for the purpose of energy efficiency [24]. The algorithm is based on the subgame perfect Nash equilibrium (SPNE) approach which is used to find the Nash equilibrium (NE) in every subgame of the real game. The selection of the CHs relies on the SPNE technique.

Romero et al. [25] examine a game theory-based strategy to reduce energy consumption in cognitive WSNs. The strategy was initially meant to provide an answer to the problem of spectrum inefficiency. The proposed technique was shown to improve energy consumption through its ability to switch communication channels. The approach makes use of a decision strategy of changing the transmission channel depending on the behaviour of the rest of the network nodes through the application of a game theoretic technique.

As presented above, most of the related works are contextualised to traditional WSN-based M2M communications. In modern times, neither the devices in a network that constitutes M2M communications are homogeneously WSNs nor do the composing nodes share the same network operator. This makes the approach for the management of cooperative communications in M2M networks to be different from how WSNs are managed. The current sequel proposes a new solution that is a modification of the coalition game theoretical clustering (CGTC) proposed by Afsar [15]. The proposed approach considers the application of coalition game theoretical clustering that invokes an incentive scheme (CGTCI). The proposed approach aims at stimulating cooperation amongst the M2M devices that are not necessarily from the same operator. The incentive paves the way for transmissions at short distances in the hierarchical partitioned network which has an overall effect of reduced energy consumption in the network.

3. Fundamentals of the Proposed Algorithm

This section presents the basics of the coalition game and radio model as fundamentals of the proposed algorithm.

3.1. Basics of Coalition Game. A coalitional game can be an ordered pair (N, V), in which N is a finite set of players referred to as the grand coalition and the characteristic function V is described as $V : 2^N \longrightarrow R$. In the coalition formation game, coalition structures which are partitions of the grand coalition N are constructed and defined as $S = \{S_1, \ldots, S_i, \ldots, S_K\}$. In our future discussions, the following properties of coalition games will be considered.

3.1.1. Individual Rationality. A player n will be a member of a coalition, only when the gains achieved by being in the coalition are more than those when acting selfishly or being a free rider. This can be expressed as $X_n > V(\{n\})$, where X_n is the utility factor of a player in a coalition and $V(\{n\})$is the utility factor of a free rider.

3.1.2. Group Rationality. The sum of the payoffs of a coalition should be at least the value of the coalition. This is represented as $\forall C \subseteq N$ and $X(C) \geq V(C)$. Here, $\forall C$ represents all the coalitions, N is the grand coalition, $V(C)$ is the value of the coalition, and $X(C)$ is the payoff to the coalition.

3.2. Radio Model. The computation of the energy consumed during data transmission from sources to the sink considers the radio model that is illustrated in Figure 1 [26]. The

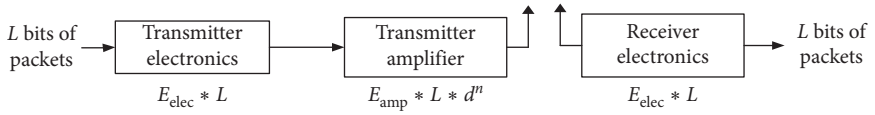

Figure 1: Radio model for energy dissipation.

energy for data transmission is proportional to distance (d) and the amount of data bits (L).

Accordingly, the energy needed to transmit L bits of data packets through distance d is expressed as

$$E_{TX}(L,d) = E_{TX(elec)}(L) + E_{TX(amp)}(L,d), \quad (1)$$

$$E_{TX}(L,d) = \begin{cases} L\left(E_{elec} + \epsilon_{fs} d^2\right), & d \le d_o, \\ L\left(E_{elec} + \epsilon_{mp} d^4\right), & d > d_o. \end{cases} \quad (2)$$

The energy expended in receiving the data packets is expressed as

$$E_{RX} = E_{RX(elec)}(L). \quad (3)$$

In equations (1) and (2), $E_{elec}(L)$ is the energy consumption required to run the transmitter circuitry for an L bit packet; $E_{TX(amp)}(L,d)$ is the energy consumed when an amplifier transmits L bits through a distance (d); ϵ_{fs} and ϵ_{mp} are the amplification energy of free space and multipath models, respectively; and the threshold d_o is expressed as $d_o = \sqrt{(\epsilon_{fs}/\epsilon_{mp})}$.

This section has presented fundamentals that will be considered during the discussion of the proposed algorithm. In the next section, the modelling of the proposed algorithm is highlighted.

4. System Model

This section presents a detailed description of the proposed system model. Consider a single cell with one BS and a set of N heterogeneous M2M devices $N = \{1, 2, \ldots n\}$ that are randomly distributed within the coverage area of the BS. To balance the load in the network, the network area is partitioned into hierarchical zones. Figure 2 shows the structural representation of the proposed system model.

Devices in the outer zones are organised into coalition structures. Each coalition structure is supervised by a CH. The CH receives, aggregates data packets of devices associated with it, and then forwards them to selected CHs/devices in the hierarchical zones. The devices in the zone closer to the BS act as gateways, and they do not join coalition structures. They receive and aggregate data packets from CHs of the outer zones and supplement them with their own before forwarding to the BS [27]. In this network, two links are defined: backhaul and access links. The latter links the inner zone devices to the BS, while the former links devices in the coalition structure to the CH.

The details of the proposed approach are presented in the following forms: network partitioning, coalition formation, and contract model-based incentive.

4.1. Creation of Network Partitions. The partitioning of the network considers the application of the Sierpinski triangle technique [28]. To achieve network partitioning, the following steps are followed:

(i) Consider the area of a single cell with BS as an equilateral triangle

(ii) Divide the triangle into four smaller congruent equilateral triangles

(iii) Repeat step (ii) with each of the remaining smaller triangles

(iv) For creation of three partitions, introduce curved lines to join bases of triangles that have contact with the major triangle

(v) Triangles in each partition represent the maximum number of subcluster heads that can be selected by the cluster head

Steps (i)–(v) described above are illustrated in Figure 3.

4.2. Formation of Coalition Structures. The formation of coalition structures starts with the generation of cluster heads in the respective zones. The devices choose the optimum cluster based on the calculated utility function.

4.3. Election of Cluster Heads (CHs). In the selection of the cluster head (CH), a device with the highest cost function is elected as a CH in each zone [29]. The elected CH plays the role of selecting sub-CHs in the zone whose cost function is above the average threshold. The parameters that determine the cost function of a device are ratio of residual to initial energy (E_r/E_{init}), trust level (T_n), node degree (Q), and device data transmission energy to the BS ($E_{TX}(L, BS)$). Their corresponding weights are given as α_1, α_2, α_3, and α_4, respectively. The cost function is defined as

$$\text{cost}(n) = \left[\alpha_1\left(\frac{E_r(t)}{E_{init}}\right) + \alpha_2 T_n + \alpha_3 Q + \alpha_4 E_{TX}(L, BS)\right](t), \quad (4)$$

where E_{init} is the initial device energy at time $t = 0$, $E_r(t)$ stands for the current device residual energy, and T_n is the device trust level. The trust level describes certainty of the relay nodes based on the success of achieving the objective of delivering data packets to the sink. $E_{TX}(L, BS)$ denotes the device transmission energy used for packet transmission to the BS. The sum of the cost weights $\alpha_1, \alpha_2, \alpha_3$, and α_4 equals unity.

4.4. Coalition Structures. The set of players in a coalition game is represented as $N = \{1, 2, \ldots, n\}$; devices elected as

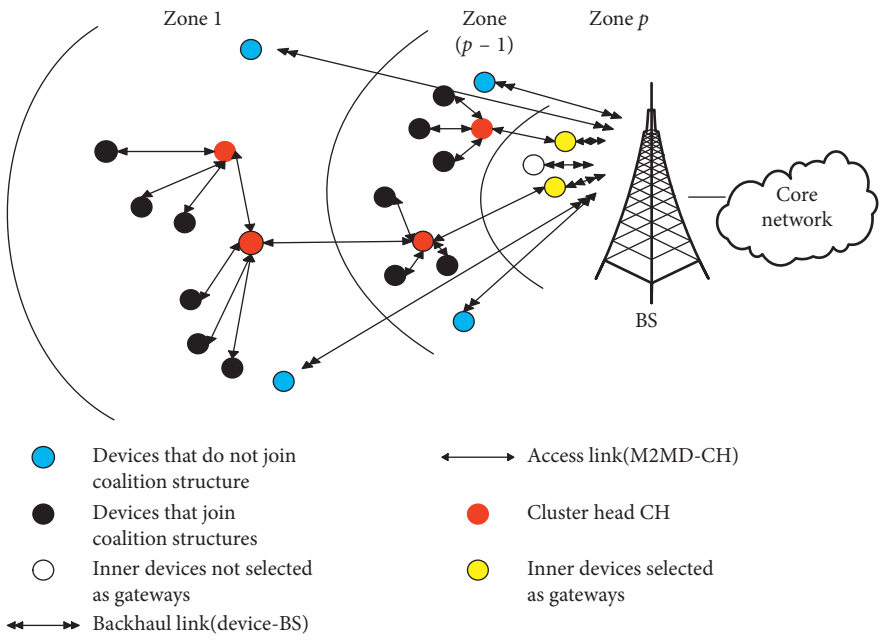

Figure 2: Structural representation of the proposed system model.

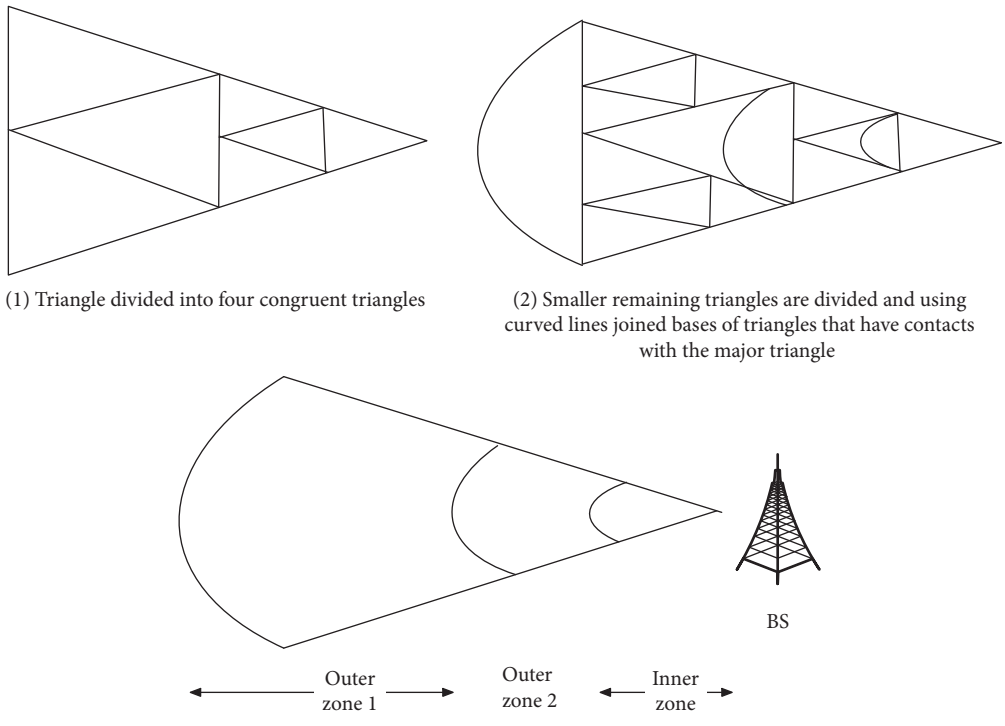

(1) Triangle divided into four congruent triangles

(2) Smaller remaining triangles are divided and using curved lines joined bases of triangles that have contacts with the major triangle

(3) Complete partitioning of a single cell with BS

Figure 3: Creation of network partitions.

cluster heads in the zones are defined as $CH_{A(i)}$ and $CH_{B(i)}$, $i = \{1, 2, \ldots, M\}$, for zones A and B, respectively. The players in these zones have an option of joining a coalition or not. In either way, it depends on the computed utility factor (U_f). A device will opt for high U_f, as this signifies less energy consumption. During the computation of U_f, energy used and interference encountered as data packets transmitted from the source to the sink are considered. The expression of U_f is given as [30]

$$U_f\left(E_{TX}(L,d),\theta_{sn}\right) = \left(\frac{R_t}{E_{TX}(L,d)}\right)\left(1-e^{-0.5sn}\right)^L, \quad (5)$$

where U_f is the utility factor of node n; E_{TX} is the energy required to transmit data packets, as given in equation (1),

and depends on distance (d) and data packets (L); θ_{sn} is the signal-to-interference-and-noise ratio (SINR) experienced by node n during data transmission; and R_t is the rate at which information is transmitted to the BS/sink. The main objective for each node is to maximise its utility factor that is determined by the distance (d), data packets (L), and SINR (θ_{sn}). The utility factor for a node joining a coalition structure (U_{fc}) having L packets, d_c distance, and θ_{snc} interference is given as [30]

$$U_{fc}\left(E_{TX}\left(L, d_c\right), \theta_{snc}\right) = \left(\frac{R_t}{E_{TX}\left(L, d_c\right)}\right)\left(1 - e^{-0.5\theta_{snc}}\right)^L. \quad (6)$$

The utility factor for a node that considers free riding has distance and interference denoted as d_{fr} and θ_{snfr}, respectively, and packets denoted as L. The utility factor of a free riding node can be expressed as

$$U_{fr}\left(E_{TX}\left(L, d_{fr}\right), \theta_{snfr}\right) = \left(\frac{R_t}{E_{TX}\left(L, d_{fr}\right)}\right)\left(1 - e^{-0.5\theta_{snfr}}\right)^L. \quad (7)$$

Different parameters in each case result in two values of utility factors being obtained. The utility factor of joining a coalition and that of free riding are compared. The option that generates a higher utility factor is selected by the device as it signifies less transmission energy and therefore energy saving.

For the nodes in the coalition structure, the respective CHs through the time-division multiple access (TDMA) establish the schedule for transmission up to the sink. In this arrangement, data to the sink are periodically transmitted. Depending on each node's computed utility factor, some nodes will assign themselves to the CH, while some will free ride. As packets are transmitted and received at the CH, energy is consumed. The computations of energy consumed during transmission and aggregation of data packets at the CH (E_{CH}) during the formation of the coalition structure and when nodes free ride to the BS/sink $E_{TX(NC)}$ are defined by equations (8) and (9), respectively. The two equations apply the energy equations of the radio model [26]:

$$\begin{aligned} E_{CH} &= Ln\left(\left(E_{ele} + \epsilon_{fs} d^2\right) + E_{RX(ele)}\right) \\ &= E_{TX(CH)} + E_{Agg(CH)}, \end{aligned} \quad (8)$$

$$E_{TX(NC)} = Ln\left(E_{ele} + \epsilon_{fs} d^4\right), \quad (9)$$

where L represents the data packet being transmitted, E_{ele} is the electronic energy, $E_{RX(ele)}$ is the electronic energy consumed as data packets are received, ϵ_{fs} denotes amplifier energy of free space, E_{Agg} is the energy consumed during the data packet aggregation, n is the number of devices (nodes) assigned to the CH, and d^2 is the distance between the CH and next hop; it could be d^4 if d is greater than the threshold d_o, and this is done based on equation (2).

4.5. Formulation of Contract-Modelled Incentive. The need to sustain cooperative communication calls for special prescription among M2M devices. The invoking of an incentive that is based on the contract-based model is proposed. This section presents the design of the incentive mechanism. The incentive design considers the work proposed in [31, 32]. The parameters that are considered by both the source and the relay devices before venturing into the contract are the basic wage (recharge energy), relay effort, and bonus. In the formulation of the contract model, the interest of both the source and relay needs to be balanced. The following sections highlight the modelling of the source and relay and contract formulation and operations.

4.6. Source Modelling. In this section, we model the optimal achievable energy saving that comes because of the use of the cooperative device in a data packet transmission. Considering the help received from the ith relay device in forwarding data devices, the total achievable energy saving by the source due to cooperation can be expressed as [33]

$$\pi_i = \Phi_i E_i + \delta, \quad (10)$$

where Φ_i is the profit of each unit of energy and is always greater than zero, E_i is the ith relay energy of transmission at the source's receiver, and δ is the random variable that follows the Gaussian distribution curve, $N(\mu, \sigma^2)$.

Considering the linear sharing scheme, the compensation W_i towards the ith relay device is formulated as [34]

$$W_i = \propto_i + \beta_i E_i, \quad (11)$$

where $\propto_i$ is the basic recharge energy of the ith zone B's relay device (basic wage) and β_i ($\beta_i \in [0, 1]$) denotes the bonus (extra recharge energy) based on performance of the relay device as an incentive. The relay devices have different abilities and actions and hence obtain different bonuses. Under cooperation, the source devices strive to achieve maximum utility. The formulation that defines the source's total utility attained with the help of the relay device considers equations (10) and (11). Source utility (U_s) is given as

$$\begin{aligned} U_s &= \sum_{i=1}^{n} \left[\pi_i - W_i\right] \\ &= \sum_{i=1}^{n} \left[\Phi_i E_i + \delta - \propto_i - \beta_i E_i\right], \end{aligned} \quad (12)$$

$$\text{with means } E\left[U_s\right] = \sum_{i=1}^{n} \left[\Phi_i E_i - \propto_i - \beta_i E_i\right], \quad (13)$$

$$\text{and variance } \mathrm{Var}\left[U_s\right] = \sum_{i=1}^{n} \left[1 - \beta\right]^2 \sigma^2. \quad (14)$$

The source's expected utility considering a constant absolute risk aversion (CARA) preference that considers equations (13) and (14) is defined as

$$E\left[U_s\right] = E\left[-e^{-\eta s U_s}\right] = e^{-\eta s\left[E\left(U_s - (1/2)\mathrm{Var}\left[U_s\right]\eta s\right)\right]}. \quad (15)$$

4.7. Relay Modelling. The devices in zones B and C are the potential relays to be incentivised in the network. The focus

is on the input effort and rewards granted to the devices that participate in multihop transmission of data packets to the sink/BS. More energy (effort) used attracts more cost paid by the relay devices. If the channel gain between the source device (SD), and the receiver device (RD) is defined as $h_{(\mathrm{SD,RD})}$ and the cost of effort used is C_iE_i and increases with effort, the device communication cost of the ith relay device is assumed to be quadratic and is expressed [32] as

$$C_i(E_i) = \frac{\left(c_i(E_i)^2\right)/2}{h_{(\mathrm{SD,RD})}}, \tag{16}$$

where c_i is the cost of energy per unit transmission of the ith relay device. From (16), the hidden information of the ith relay device that depends on the cost of energy of transmission and the channel gains between the source and the receiver can be formulated. The hidden information (battery, memory, and computing power) can be expressed as

$$\theta_i = \frac{c_i}{h_{(\mathrm{SD,RD})}}. \tag{17}$$

When θ_i is low, it means the channel condition of the ith relay device is good, and vice versa.

The presentation of payment by the source device to the ith relay device considers equations (11) and (16) and is defined linearly as [34]

$$W_{i(\mathrm{RD})} = \propto_i + \beta_i E_i - C_i E_i. \tag{18}$$

In the payment offered by the source, bonuses towards the ith relay device are different and follow normal distribution with means that take the following form [32]:

$$E\left[W_{i(\mathrm{RD})}\right] = \propto_i + \beta_i \Phi_i E_i - C_i E_i, \tag{19}$$

$$\mathrm{Var}\left[W_{i(\mathrm{RD})}\right] = \beta_i^2 \sigma^2. \tag{20}$$

If the ith relay device adopts a constant absolute risk aversion (CARA) preference, then the ith device's (RD (receiver device)) utility is expressed as

$$U\left(W_{i(\mathrm{RD})}\right) = e^{-\eta_{\mathrm{RD}} W_{i(\mathrm{RD})}} \tag{21}$$

The expected utility for the ith relay device can be expressed as

$$\begin{aligned} E\left[U\left(W_{i(\mathrm{RD})}\right)\right] &= E\left[e^{-\eta_{\mathrm{RD}} W_{i(\mathrm{RD})}}\right] \\ &= \frac{-1}{\sqrt{2\prod \mathrm{Var}\left[W_{i(\mathrm{RD})}\right]}} \int_{-\alpha}^{\alpha} e^{-\left(\left(\left(R_N\right)^2 - 2E\left[W_{i(\mathrm{RD})}\right]W_{i(\mathrm{RD})} + \left(E\left[W_{i(\mathrm{RD})}\right]^2\right) + 2\mathrm{Var}\left[R_N\right]\eta\mathrm{RD}R_N\right)/\left(2\mathrm{Var}\left[W_{i(\mathrm{RD})}\right]\right)\right) dW_{i(\mathrm{RD})}} \\ &= -e^{-\eta\mathrm{RD}\left[E\left[W_{i(\mathrm{RD})}\right]\right] - (1/2)\mathrm{Var}\left[W_{i(\mathrm{RD})}\right]\eta\mathrm{RD}} \\ &= -e^{-\eta\mathrm{RD}\left[\propto_i + \beta_i\Phi_i E_i - C_i E_i - ((\eta\mathrm{RD})/2)\beta_i^2\sigma^2\right]}. \end{aligned} \tag{22}$$

4.8. Relay Incentive Mechanism. This section defines the design of contract-modelled incentive between the source device and relay device. The contract formulation considers the monopolistic design technique where the source device proposes a contract item (α_i, E_i) that is acceptable by the relay device [32]. In this work, it is assumed that the source knows the ability and action of the existing relay devices (symmetric information). The design will enable the source achieve utility of the relay that is maximum, which when considered under any network information scenario is the upper bound of the source's achievable utility. Under the symmetric information scenario, maximising the expected source utility, equation (15) requires that individual rationality (IR) is satisfied. This can be attained through the derivation starting from

$$\begin{aligned} &\max_{\{\{E_i\alpha_i\}\geq 0\}} \quad E[U_s], \\ &\text{s.t. (IR)} \quad \alpha_{i+}\beta_i\Phi_i E_i - C_i E_i - \frac{\eta\mathrm{RD}}{2}\beta_i^2\sigma^2 \geq \widehat{u}, \quad 1 \leq i, \leq n, \end{aligned} \tag{23}$$

where $\widehat{u}$ is called the retained utility, the minimum utility level for the source during contract formulation.

Let

$$\begin{aligned} \mathrm{fs} &= E[U_s] - \frac{\mathrm{Var}[U_s]\eta s}{2}, \\ &= \sum_{i=1}^{n}\left[\Phi_i E_i - W_i - \frac{\eta s\sigma^2}{2}\left(1-\beta'\right)^2\right]. \end{aligned} \tag{24}$$

The optimisation problem in equation (18) can be written as

$$\begin{aligned} &\max_{\{\{E_i\alpha_i\}\geq 0\}} \quad \mathrm{fs} = \sum_{i=1}^{n}\left[\Phi_i E_i - W_i - \frac{\eta s\sigma^2}{2}\left(1-\beta'\right)^2\right], \\ &\text{s.t (IR)} \quad \alpha_{i+}\beta_i\Phi_i E_i - C_i E_i - \frac{\eta R\ D}{2}\beta_i^2\sigma^2 \geq \widehat{u}, \quad 1 \leq i, \leq n. \end{aligned} \tag{25}$$

Considering that there exists an optimal contract item $(\alpha_i, E_{A(i)})$ that solves the equation $\alpha_{i+}\beta_i\Phi_i E_i - C_i E_i - (\eta\mathrm{RD}/2)\beta_i^2\sigma^2 \geq \widehat{u}$, the source can obtain maximum utility by

decreasing α_i until the relay device attains the retained utility defined as

$$\alpha_{i+}\beta_i\Phi_i E_i - C_i E_i - \frac{\eta \mathrm{RD}}{2}\beta_i^2\sigma^2 = \widehat{u}. \tag{26}$$

Considering equation (26), the source's expected utility maximisation problem in equation (25) can be simplified as

$$\max_{\{\{E_i\}\geq 0\}} = \sum_{i=1}^{n}\left[\Phi_i E_i - \widehat{u} - C_i E_i - \frac{\eta \mathrm{RD}}{2}\beta_i^2\sigma^2 - \frac{\eta s\sigma^2}{2}\left(1-\beta_i\right)^2\right]. \tag{27}$$

The source optimisation problem that had two variables $\{E_i, \alpha_i\}$ in (25) is simplified to that with one variable $\{E_i\}$ in (27), which can be computed by interior point techniques [35]. A summary of the operation of contract incentive mechanism can be explained as follows.

The set of source devices, set of relay devices, and set of contract items (energy credits) from the source assumed to be cluster heads are represented as CH_i, $i = \{1, 2 \ldots M\}$, RD_S, $S = \{1, 2 \ldots P\}$, and E_i, respectively. The CH_i always strives to maximise E_i, where minimum energy credits are availed to the RDs; this helps CH_i to minimise its energy expenditure so as to stay in operation for an elevated period. The operation of a contract incentive mechanism starts with the source device broadcasting the contract item (E_i) to the relay devices (RDs). RDs evaluate the E_i, and the RD that accepts the broadcasted E_i gives feedback. Once CH_i receives a feedback from RDs, it passes the cooperative instructions and required data packets for transmissions. The RDs receive and aggregate the data packets and supplement them with their own and forward to the processing unit/sink. The CH_i rewards RDs with the agreed E_i after successful delivery of the data packets. The operation is illustrated in Algorithm 1.

This section has described the parts of the proposed system model. The next section presents the proposed algorithm CGTCI.

5. Coalition Game Theoretical Clustering with Incentive (CGTCI) Algorithm

This section gives a description of the proposed algorithm and analysis of energy consumption during data packet transmissions.

5.1. Description of CGTCI Algorithm. It is assumed that the network area is partitioned into three hierarchical zones: A, B, and C, with coalition structures forming in zones A and B, while devices in zone C communicate directly with the BS. Election of CHs in zones A and B is performed by considering equation (4). A device of high cost function in the zone is elected as a CH. For zone A, the elected CH selects more devices of high cost function to be sub-CHs to constitute their coalitions. The number of devices selected as sub-CHs should not exceed the number of triangles in the partition. Other devices within the zone not selected as CHs have an option of joining a coalition or communicating directly to the BS. This is determined by the utility factor of a device that is computed by equations (6) and (7). A high computed utility factor means less energy consumption by the device. When devices get associated with specific CHs in the zone, coalition structures are generated. The devices forward their data packets to respective CHs in the coalition structures in the zones. The CHs, which are the source device, present the contract items $(\alpha_i, E_i\}$ to the relay device with expected maximum utility of the source. This is derived through equations (23)–(27). The relay devices evaluate the contract items based on their expected utility derived through equations (19)–(22). The relay devices that accept the contract items receive and aggregate the packets and transmit to the BS/sink. The flow diagram in Figure 4 illustrates the proposed CGTCI algorithm. The steps of the flow diagram are summarised as follows:

(i) The Sierpinski triangle technique is applied in partitioning the network area into hierarchical zones A, B, and C. The technique helps in the formation of unequal coalition structures that solve the problem of hot spots.

(ii) Coalition structures are formed after election of CHs.

(iii) Contract-modelled incentive is invoked to stimulate multihop transmissions among the devices in the hierarchical partitioned zones to the BS. A balance is struck between the utility of the source device and the individual rationality (IR) of the potential relay devices at the time of implementing the incentive parameter. An optimal incentive is offered as a contract item to the potential relay devices. The incentive provokes transmissions of data packets through short distances up to the BS and contributes to minimisation of energy consumption in the network.

5.2. Analysis of Energy Consumption Process. The computation of energy consumption applies equations (8) and (9) discussed in Section 4. In this work, for the devices that embrace formation of coalition structures, energy is expended in the following ways: (1) as data packets are transmitted to the CH $(E_{\mathrm{TX(CH)}})$, (2) during data packet aggregation at the CH $(E_{\mathrm{Agg(CH)}})$, and (3) as aggregated data packets are transmitted to the next hop in the next zone/BS $(E_{\mathrm{TX(NH)}})$. For the devices that opt for the noncoalition approach, where devices individually transmit data packets to the BS, the energy used for transmission is denoted as $(E_{\mathrm{TX(NC)}})$. For the zones far from the BS, the total energy consumed at the time (t) can be computed using the expression

$$E_Z(t) = \left(E_{\mathrm{TX(CH)}} + E_{\mathrm{Agg(CH)}} + E_{\mathrm{TX(NH)}} + E_{\mathrm{TX(NC)}}\right)(t). \tag{28}$$

From (28), the computation of energy consumed in zones A $(E_{Z(A)})(t)$, B $(E_{Z(B)})(t)$, and C $(E_{Z(C)})(t)$ can, respectively, be derived from the following expressions:

```
(1) Initialise CH_i, RD_s, and E_i
(2) for i = 1 : M
(3)     CH_i broadcast (E_i)
(4)     For s = 1 : P
(5)         if RD_s accept (E_i) = true then
(6)             RD_s send (RD_s feedback, to CH_i)
(7)             CH_i send (cooperative instructions and relay data packets, to RD_s)
(8)             RD_s data packets ⟵ aggregate (RD_s relay data packets)
(9)             RD_s data packets ⟵ concatenate (RD_s relay data packets, RD_s own data)
(10)            RD_s send (RD_s data packets, to sink)
(11)            if cooperative Transmission fail = false then
(12)                CH_i reward (RD_s)
(13)            else
(14)                CH_i no reward (RD_s)
(15)            end
(16)        else
(17)            go to step (4)
(18)        end
(19)    end
(20) end
```

Algorithm 1: Operation of contract incentive mechanism.

$$E_{Z(A)}(t) = \left(E_{\mathrm{TX(CH)}[A]} + E_{\mathrm{Agg(CH)}[A]} + E_{\mathrm{TX(NH)}\{B\}} + E_{\mathrm{TX(NC)}[A]\{\mathrm{BS}\}}\right)(t), \tag{29}$$

$$E_{Z(B)}(t) = \left(E_{\mathrm{TX(CH)}[B]} + E_{\mathrm{Agg(CH)}[B]} + E_{\mathrm{Agg(RD)}[A+B]} + E_{\mathrm{TX(NH)}\{C\}} + E_{\mathrm{TX(NC)}[B]\{\mathrm{BS}\}}\right)(t), \tag{30}$$

$$E_{Z(C)}(t) = \left(E_{\mathrm{Agg(RD)}[A+B+C]} + E_{\mathrm{TX(NH)}\{\mathrm{BS}\}} + E_{\mathrm{TX(NRD)}[C]\{\mathrm{BS}\}}\right)(t), \tag{31}$$

where $E_{\mathrm{TX(CH)}[A]}$ and $E_{\mathrm{TX(CH)}[B]}$ denote energy consumed as data packets are transmitted to the CHs in zones A and B, respectively; $E_{\mathrm{Agg(CH)}[A]}$, $E_{\mathrm{Agg(CH)}[B]}$, and $E_{\mathrm{Agg(RD)}[A+B+C]}$ denote energy consumed during data aggregation at CHs in zones A and B and at the relay device in zone C, respectively; $E_{\mathrm{TX(NH)}\{B\}}$, $E_{\mathrm{TX(NH)}\{C\}}$, and $E_{\mathrm{TX(NH)}\{\mathrm{BS}\}}$ denote energy consumed as data packets are transmitted to the next hop B, C, and BS, respectively; and $E_{\mathrm{TX(NC)}[A]\{\mathrm{BS}\}}$, $E_{\mathrm{TX(NC)}[B]\{\mathrm{BS}\}}$, and $E_{\mathrm{TX(NRD)}[C]\{\mathrm{BS}\}}$ represent energy consumed from devices in zones A and B that are not organised in coalition structures as they transmit data packets to the BS and devices in zone C that are not selected as relay devices as they transmit data packets to the BS.

Total energy consumed in one round of data packet transmission to the BS at the time (t) is obtained as a summation of energies defined in equations (29)–(31):

$$E_T(t) = \left(E_{Z(A)} + E_{Z(B)} + E_{Z(C)}\right)(t). \tag{32}$$

This section has highlighted the proposed CGTCI algorithm and how energy consumed in one round of data packet transmission is computed. In the next section, performance evaluation of the algorithm is presented.

6. Performance Evaluation

This section presents the simulation parameters, scenarios, and results.

6.1. Simulation Parameters. The simulation of the CGTCI is carried out in the MATLAB software environment. Three parameters are considered: total energy trend in the network, energy trend for the farthest located device from the BS, and number of surviving devices in relation to the number of rounds of packet transmissions. 200 devices are considered, and the BS is located at (10,000, 10,000) metres. It is assumed that packets are all delivered successfully to their respective destinations, and interference in the network is assumed to be fixed and equal for all the nodes. The CGTCI algorithm is evaluated for energy efficiency, and it is compared with CGTC [15], CG-DC that is developed from the improved low-energy adaptive clustering hierarchy (LEACH) [16], and noncoalition game (NCG) algorithms. The total initial energy in the system is 2300 joules. Table 1 presents other parameters utilised in the simulation that are comparable to those presented in [15].

6.2. Simulation Scenarios. The data transmission scenarios for NCG, CGTC/CGTCI, and CG-DC algorithms are presented in the following sections.

6.3. NCG Simulation Scenario. Figure 5 illustrates the NCG simulation scenario where each device transmits its own data packets to the BS.

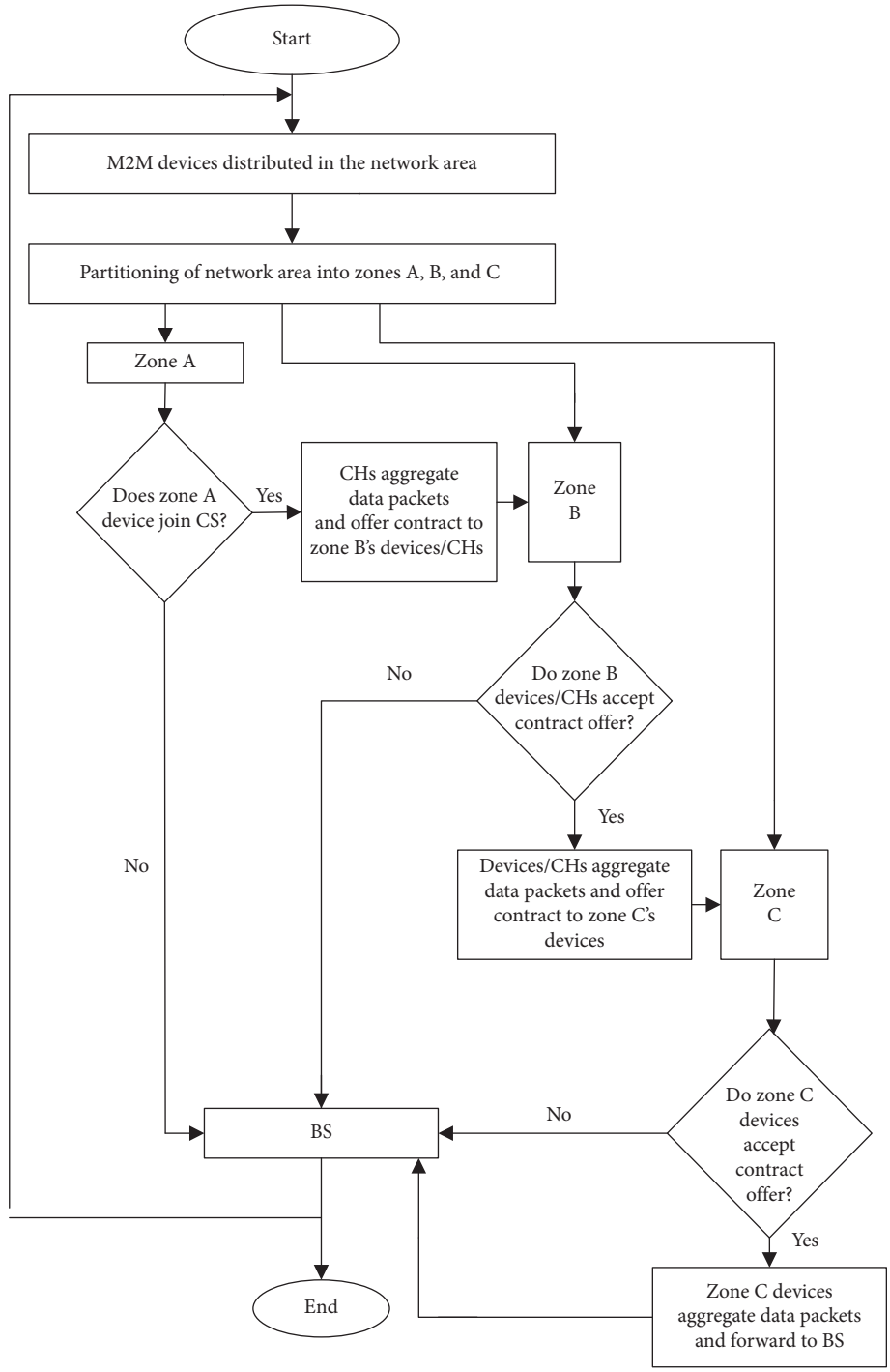

Figure 4: Flow chart of the CGTCI algorithm.

6.4. CGTC/CGTCI Simulation Scenario. CGTC and CGTCI have a similar structural arrangement that is shown in Figure 6. In the outer and middle zones, the main CH is elected, which then selects other sub-CHs whose cost functions are above the average threshold. The inner zone devices are not organised in coalition structures. The devices in the outer and middle zones then apply the utility equations (6) and (7) to select specific CHs in the zone where their utility factor score is the highest. The CGTCI algorithm has data packet transmission from three regions: the inner, middle, and outer zones. (i) For the inner zone, the devices communicate directly with the BS. (ii) For the middle zone, after the CHs aggregate data packets of their members, they invoke a contract-modelled incentive. The CHs broadcast their contract items to the inner zone devices, and the contract items are evaluated. Those that accept the contract items receive and aggregate the data packets, which they forward to the BS. (iii) For the outer zone, first there is an

Table 1: Simulation parameters.

Parameter	Value	Description
N	200	Number of nodes
BS (location)	(10,000, 10,000)	Location of BS in metres
BS (cov.)	14,000 m	Radius of BS coverage
L	0–1000	Data payload in bits (varying)
ϵ_{fs}	$1 * 10^{-12}$ J/bit/m^2	Amplification energy of free space
$\boldsymbol{\epsilon}_{\text{tr}}$	$1.3 * 10^{-15}$ J/bit/m^4	Amplification energy of multipath
En/b	$50 * 10^{-9}$ J	Energy/bit
$E_{\text{agg.}}$	$5 * 10^{-9}$ J	Data aggregation energy
d_o	87 m	Threshold value ($\sqrt{(\epsilon_{\text{fs}}/\epsilon_{\text{mp}})}$)
E_i	0–20 joules	ith relay energy from the source (incentive energy)
E_D	0–20 joules	Device energy

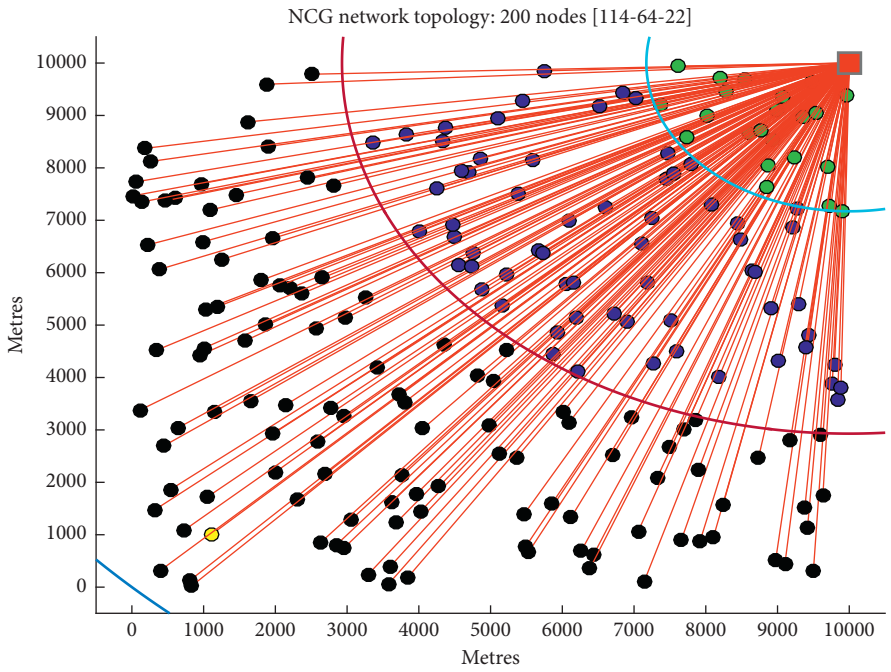

Figure 5: NCG simulation scenario.

internal multihop transmission of data packets, where the specific sub-CHs after receiving and aggregating data packets of their members establish a route through other sub-CHs in the zone until they reach the main CH. The main CHs aggregate the data packets and broadcast the contract items to the devices in the middle zone. The device in the middle zone that accepts the contract items repeats the procedures in (ii). For the CGTC algorithm, the operation is like the procedures of CGTCI but lacks the engagement of the incentive.

6.5. CG-DC Simulation Scenario. Figure 7 illustrates the simulation scenario of coalition game-direct communication (CG-DC). In this arrangement, elected CHs receive data packets from members of the coalition structure and forward them directly to the BS, with no multihop communication.

6.6. Simulation Results. This section describes sample simulated results, and energy efficiency of the algorithms is defined based on the following:

(i) The trend of computed average energy remaining in the network as the number of rounds of packet transmissions increases

(ii) The trend of computed average energy in the network for the devices located in the farthest zone from the BS as the number of rounds of packet transmissions increases

(iii) The trend of computed average energy in the network for the devices located in the zone closest to the BS

(iv) The number of nodes remaining in the network as the number of rounds of data packet transmissions increases

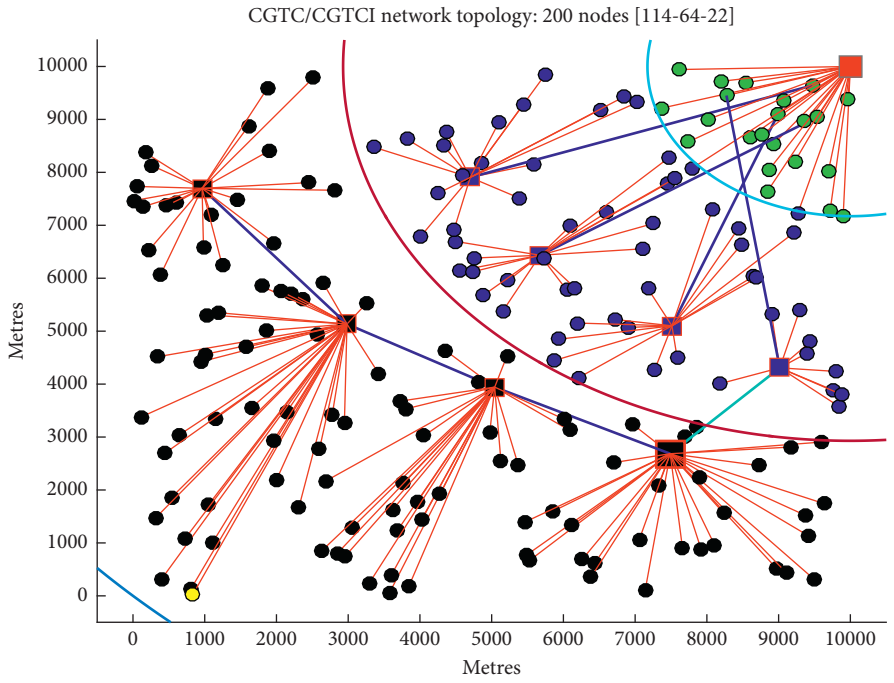

Figure 6: CGTC/CGTCI simulation scenario.

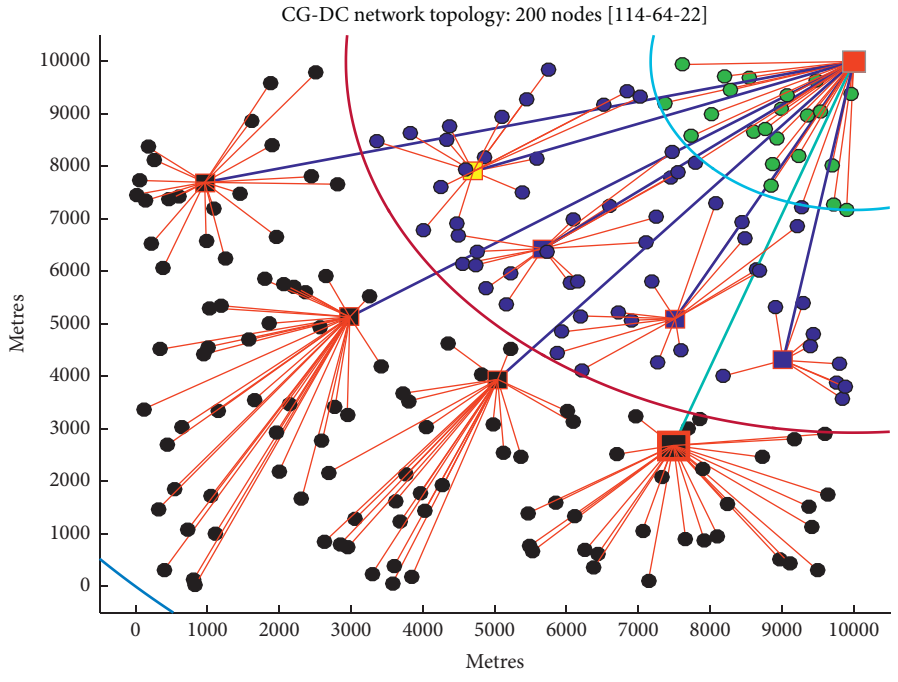

Figure 7: CG-DC simulation scenario.

6.6.1. Trend of Total Energy Remaining in the Network. Figure 8 shows that as the number of rounds of packet transmissions increases, there is a steep decrease in energy in NCG when compared with CGTC, CG-DC, and CGTCI. The decrease in energy displayed by the CGTCI algorithm is less when compared with CGTC, CG-DC, and NCG. At the 5000th round of packet transmission, when the NCG algorithm has approximately 0% remaining energy in the network, CGTCI has approximately 20% remaining energy, while CGTC and CG-DC display approximately 10% energy remaining in the network. Figure 9 displays the percentages of the remaining energy at the 5000th round of packet transmission with NCG as a reference. The observation is attributed to the engagement of a contract-modelled incentive which stimulates the devices in the respective zones to accept a multihop mode of transmissions. This enables

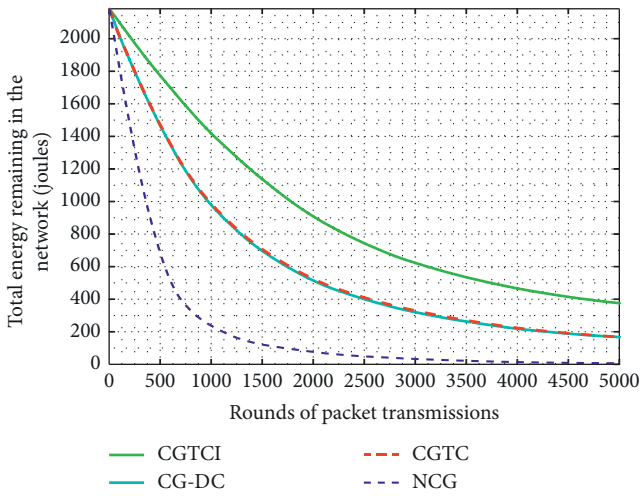

Figure 8: The trend of total energy remaining in the network.

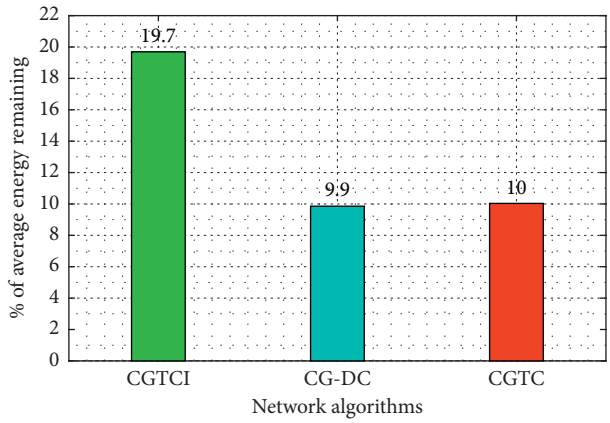

Figure 9: % of average remaining energy.

data packets to be moved from the outer zones to the BS through short-distance transmissions, consuming less energy. The network design that considers the CGTC algorithm subjects its inner zone devices (zone C) to heavy energy drain as it receives and forwards data packets to the sink. The inner zone devices are not compensated for the heavy work they do and therefore become eliminated. In the CG-DC algorithm, outer zone devices (zones A and B) drain a lot of energy as they transmit data packets through long distances to the BS, and there is no multihop transmission. NCG displays a steep decrease in the remaining energy than all the given algorithms. This is attributed to the high energy consumption in the far located devices as they transmit data to the BS. Interferences and collisions experienced during the time of transmission and accessing the BS also contribute to high energy consumption in the NCG algorithm.

6.6.2. Energy Trend for the Devices Located Farthest from the BS. Figure 10 compares the trend of the remaining energy for a cluster of devices located in the farthest zone from the BS. The trend of the remaining energy in the devices is analysed when each of the following network designs: CGTCI, CGTC, CG-DC, and NCG, is considered during data packet transmissions in a given period of simulation. With the initial energy of the device at 16.5 joules, the average remaining energy for devices sampled at 50th, 100th, 150th, and 200th rounds of packet transmissions is 95%, 93%, 92%, and 88.5% for CGTCI, CGTC, CG-DC, and NCG, respectively. This indicates that the CGTCI algorithm is 2%, 3%, and 6.5% better than CGTC, CG-DC, and NCG, respectively.

The formation of the coalition structure in CGTCI and the invoking of a contract-modelled incentive scheme pave way for the short-distance transmissions on the network up to the sink/BS. The short-distance transmission reduces energy consumption, which makes the CGTCI algorithm suitable for devices located farthest from a BS in M2M communications. Multihop transmissions are observed in CGTC; however, lack of incentive does not guarantee that the next hop is necessarily of the shortest distance. This makes the remaining energy level for the device considered under CGTC design to be lower than that when the device is considered under CGTCI design. For the CG-DC algorithm, the device's remaining energy level is slightly lower than that in CGTC but higher than that in the NCG algorithm. The farthest located device in the NCG algorithm experiences a steady decline in the energy level. The data are transmitted through a long distance and result in high energy consumption.

6.6.3. Energy Trend for the Devices Located Closest to the BS (Inner Zone). The trend of the remaining energy in the devices located close to the BS is as shown in Figure 11. The performance of the CGTCI algorithm is better than that of CGTC, CG-DC, and NCG algorithms. At the end of the simulation period, the CGTCI algorithm displays a higher level of remaining energy. This is due to the contract-modelled incentive operation invoked in the CGTCI algorithm that enables compensation of energy used by the devices selected as relays. For the CG-DC algorithm, the energy trend is gradual, but it is at a higher level than that in NCG at the end of the simulation period. This is due to the formation of coalition structures in CG-DC that are supervised by cluster heads. This helps to minimise the number that can access the sink/BS in the CG-DC algorithm when compared to the NCG algorithm and therefore assists to reduce energy loss due to collision. For the NCG algorithm, the high number of devices that try to access the sink/BS results in collision and hence energy loss. Therefore, apart from losing energy due to the transmission of data packets to the BS, energy is also lost during resending of data packets lost through collision. This makes the remaining energy level of the NCG algorithm to be lower than that of the CG-DC algorithm but higher than that of the CGTC algorithm.

For CGTC, the lack of incentive scheme means that the devices selected as relay devices do not compensate for the energy used in relaying. Therefore, the selected devices closer to the BS become exhausted much earlier. The heavy drain of energy from the devices that act as relays contributes to the

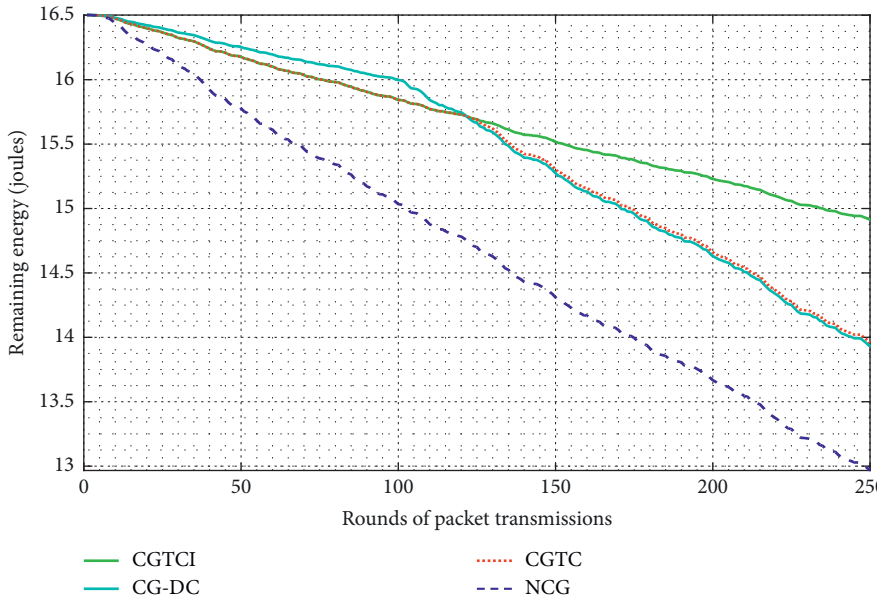

Figure 10: Trend of the remaining energy for the devices located farthest from the BS.

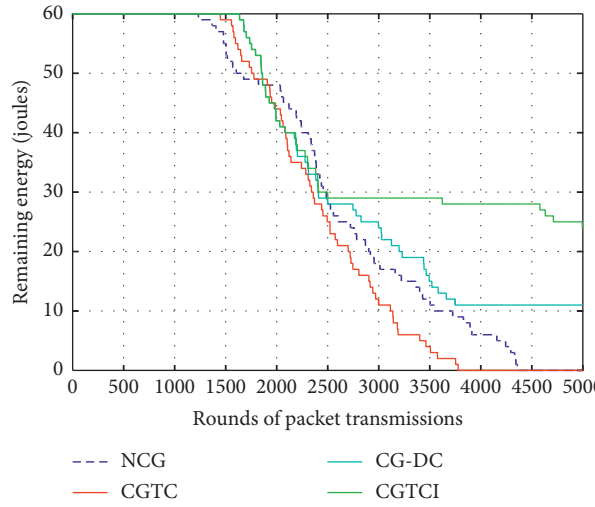

Figure 11: Energy trend for the devices located closest to the BS.

trend of the remaining energy for the devices closer to the BS in the CGTC algorithm to be lower than that in all the algorithms by the end of the simulation period. From the observation above, the CGCTI algorithm presents energy-efficient results for the devices located closer to the BS than its closely related algorithms—CGTC, CG-DC, and NCG.

6.6.4. Number of Surviving Devices in the Network. The number of surviving devices (nodes) decreases in all the algorithms as the number of rounds of transmissions increases. However, CGTCI has a higher number of surviving nodes when compared with CGTC, CG-DC, and NCG at any given round of packet transmission. Figure 12 displays the number of surviving devices against rounds of packet transmissions. The incentive scheme adopted in the CGTCI algorithm that is absent in CGTC, CG-DC, and NCG enables it to have a balanced energy consumption. As a result, the death rate of devices in the network that adopts the CGTCI algorithm in the design is reduced. The network design that applies the NCG technique posts poor results in terms of the number of surviving devices against the number of rounds of packet transmissions when compared with CGTCI. At the 5000th round of packet transmission, CGTCI has 45, CGTC and CG-DC have 20, and NCG has 0 numbers of surviving devices out of the initial 200. This translates to 22.5%, 12.5%, and 0% number of surviving devices for CGTCI, CGTC and CG-DC, and NCG, respectively. The number of surviving devices reduces at a fast rate in the network design that applies the NCG design. This is due to high energy consumption by the devices as they transmit data packets through a long distance to the BS. CGTC and CG-DC

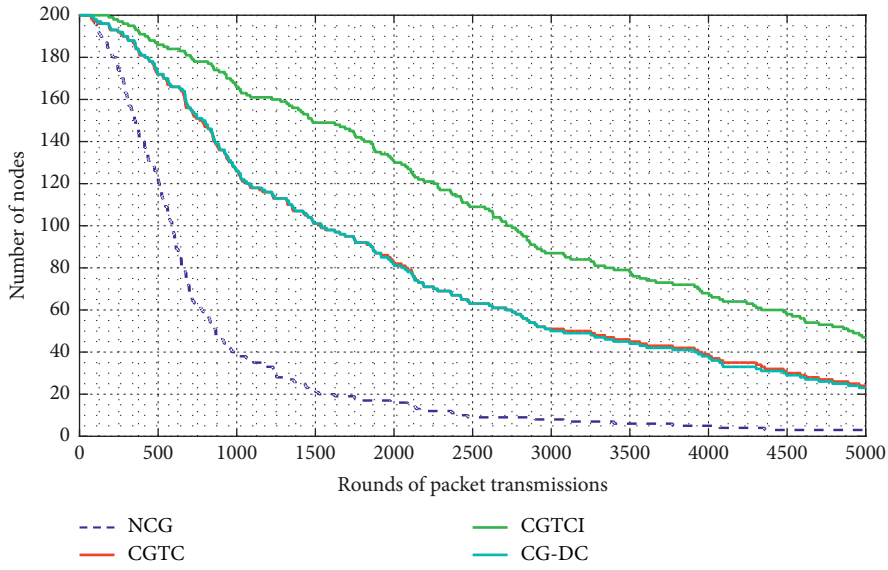

Figure 12: Trend of the number of surviving devices in the network.

display almost similar performance. In the CGTC algorithm, the creation of hot spot areas in zone C contributes to high elimination of devices. In the CG-DC algorithm, the lack of multihop transmission means that devices located far from the BS consume more energy during data transmissions and therefore die early.

7. Conclusions and Future Work

A coalition game theoretical clustering with incentive (CGTCI) was proposed for M2M communications. The main strategy was to prolong the network lifetime by controlling the energy consumption as devices transmit data packets to the BS. The network was partitioned into three zones with the help of the Sierpinski triangle. Coalition structures were formed in zones A and B, while in zone C, the devices free ride to the BS. A contract-based model incentive scheme to stimulate cooperation is invoked. The simulation results indicate that the CGTCI algorithm is better since it has, on average, 10% more remaining energy and number of surviving devices than its closely related algorithm, CGTC, at the end of simulations. From the displayed results, the CGTCI algorithm is suitable for an energy-efficient M2M communication. Being an energy-efficient algorithm, CGTCI can help maintain the required quality of service for an elevated period than CGTC.

As a further improvement of this work, the CH selection approach will be examined to optimize both time and energy that arises due to signalling. There is also a need to investigate the reliability and latency of the algorithm to ascertain its performance in packet delivery to its required destinations.

Data Availability

The data used to support the findings of this study are included within the article.

Conflicts of Interest

Regarding the publication of this research article, the authors declare that they have no conflicts of interest.

Acknowledgments

The authors would like to thank the French South African Institute of Technology (F'SATI) and the Tshwane University of Technology for their material and financial support during the production of this work.

References

[1] H. Zhou, H. Wang, X. Chen, X. Li, and S. Xu, "Data offloading techniques through vehicular ad hoc networks: a survey," *IEEE Access*, vol. 6, pp. 65250–65259, 2018.

[2] C.-M. Huang, Y.-F. Chen, S. Xu, and H. Zhou, "The vehicular social network (VSN)-Based sharing of downloaded geo data using the credit-based clustering scheme," *IEEE Access*, vol. 6, pp. 58254–58271, 2018.

[3] J. W. Raymond, T. O. Olwal, and A. M. Kurien, "Cooperative communications in machine to machine (M2M): solutions, challenges and future work," *IEEE Access*, vol. 6, pp. 9750–9766, 2018.

[4] T. O. Olwal, K. Djouani, and A. M. Kurien, "A survey of resource management toward 5G radio access networks," *IEEE Communications Surveys & Tutorials*, vol. 18, no. 3, pp. 1656–1686, 2016.

[5] D. Lin and Q. Wang, "A game theory based energy efficient clustering routing protocol for WSNs," *Wireless Networks*, vol. 23, no. 4, pp. 1101–1111, 2017.

[6] R. B. Myerson, *Game Theory: Analysis of Conflict*, Harvard University Press, Cambridge, MA, USA, 1997.

[7] P. Raja and P. Dananjayan, "Game theory-based efficient energy consumption routing protocol to enhance the lifetime of WSN," *International Journal of Information and Communication Technology*, vol. 8, no. 4, pp. 357–370, 2016.

[8] F. Li, G. Chang, L. Yao, and F. Gao, "Cooperative gamebased routing approach for wireless sensor network," *International*

Journal of Computer Applications in Technology, vol. 44, no. 2, pp. 101–108, 2012.

[9] W. Saad, Z. Han, M. Debbah, A. Hjorungnes, and T. Basar, "Coalitional game theory for communication networks: a tutorial," *IEEE Signal Processing Magazine*, vol. 26, no. 5, pp. 77–97, 2009.

[10] G. Bacci, S. Lasaulce, W. Saad, and L. Sanguinetti, "Game theory for networks: a tutorial on game-theoretic tools for emerging signal processing applications," *IEEE Signal Processing Magazine*, vol. 33, no. 1, pp. 94–119, 2016.

[11] T. AlSkaif, M. G. Zapata, and B. Bellalta, "Game theory for energy efficiency in wireless sensor networks: latest trends," *Journal of Network and Computer Applications*, vol. 54, pp. 33–61, 2015.

[12] A. C. Voulkidis, M. P. Anastasopoulos, and P. G. Cottis, "Energy efficiency in wireless sensor networks: a game-theoretic approach based on coalition formation," *ACM Transactions on Sensor Networks (TOSN)*, vol. 9, no. 4, pp. 1–27, 2013.

[13] D. B. Johnson and D. A. Maltz, "Dynamic source routing in ad hoc wireless networks," in *Mobile Computing*, pp. 153–181, Springer, Berlin, Germany, 1996.

[14] P. Michiardi and R. Molva, "Simulation-based analysis of security exposures in mobile ad hoc networks," in *Proceedings of the European Wireless Conference*, pp. 15–17, Florence, Italy, September 2002.

[15] M. Afsar, "Energy-efficient coalition formation in sensor networks: a game-theoretic approach," https://arxiv.org/abs/1512.08019.

[16] J. Xu, N. Jin, T. Peng, and Q. Zhou, "Improvement of LEACH protocol for WSN," in *Proceedings of the 2012 9th International Conference on Fuzzy Systems and Knowledge Discovery, FSKD 2012*, pp. 2174–2177, Chongqing, China, May 2012.

[17] L. Yang, Y. Z. Lu, Y. C. Zhong, X. G. Wu, and S. J. Xing, "A hybrid, game theory based, and distributed clustering protocol for wireless sensor networks," *Wireless Networks*, vol. 22, no. 3, pp. 1007–1021, 2016.

[18] K. Yue, J. Zhang, J. Li, T. Wu, and W. Liu, "A theoretic approach for prolonging lifetime of wireless sensor networks based on the coalition game model," *International Journal of Distributed Sensor Networks*, vol. 10, no. 6, article 328710, 2014.

[19] T. Wu, K. Yue, W. Liu, and J. Xu, "An energy-efficient data transfer model of wireless sensor networks based on the coalitional game theory," in *Proceedings of the Eighth International Conference on Fuzzy Systems and Knowledge Discovery (FSKD)*, pp. 1354–1358, Shanghai, China, July 2011.

[20] H. Jing and H. Aida, "Cooperative clustering algorithms for wireless sensor networks," in *Smart Wireless Sensor Networks*, InTech, London, UK, 2010.

[21] X.-N. Miao and G. Xu, "Cooperative differential game model based on trade-off between energy and delay for wireless sensor networks," *Annals of Operations Research*, vol. 206, no. 1, pp. 297–310, 2013.

[22] D. W. K. Yeung and L. A. Petrosjan, *Cooperative Stochastic Differential Games*, Springer Science & Business Media, Berlin, Germany, 2006.

[23] L. Tan, S. Zhang, and J. Qi, "Cooperative cluster head selection based on cost sharing game for energy-efficient wireless sensor networks," *Journal of Computational Information Systems*, vol. 8, no. 9, pp. 3623–3633, 2012.

[24] M. Mishra, CR. Panigrahi, and J. L. Sarkar, "GECSA: a game theory based energy efficient cluster-head selection approach in wireless sensor networks," in *Proceedings of the 2015 International Conference on Man and Machine Interfacing (MAMI)*, pp. 1–5, Bhubaneswar, India, December 2015.

[25] E. Romero, J. Blessa, A. Araujo, and O. Nieto-Taldriz, "A game theory based strategy for reducing energy consumption in cognitive WSN," *International Journal of Distributed Sensor Networks*, vol. 10, no. 1, article 965495, 2014.

[26] W. R. Heinzelman, A. Chandrakasan, and H. Balakrishnan, "Energy-efficient communication protocol for wireless micro sensor networks," in *Proceedings of the 33rd Annual Hawaii International Conference on System Sciences*, p. 10, Maui, HI, USA, January 2000.

[27] L. Liang, L. Xu, B. Cao, and Y. Jia, "A cluster-based congestion-mitigating access scheme for massive M2M communications in internet of things," *IEEE Internet of Things Journal*, vol. 5, no. 3, pp. 2200–2211, 2018.

[28] A. B. F. Guiloufi, N. Nasri, and A. Kachouri, "An energy-efficient unequal clustering algorithm using Sierpinski Triangle for WSNs," *Wireless Personal Communications*, vol. 88, no. 3, pp. 449–465, 2016.

[29] W. B. Heinzelman, A. P. Chandrakasan, and H. Balakrishnan, "An application-specific protocol architecture for wireless micro sensor networks," *IEEE Transactions on Wireless Communications*, vol. 1, no. 4, pp. 660–670, 2002.

[30] F. Kazemeyni, E. B. Johnsen, O. Owe, and I. Balasingham, "Group selection by nodes in wireless sensor networks using coalitional game theory," in *Proceedings of the 2011 16th IEEE International Conference on Engineering of Complex Computer Systems*, pp. 253–262, Las Vegas, NV, USA, April 2011.

[31] N. Zhao, M. Wu, W. Xiong, and C. Liu, "Cooperative communication in cognitive radio networks under asymmetric information: a contract-theory based approach," *International Journal of Distributed Sensor Networks*, vol. 2015, pp. 1–11, 2015.

[32] N. Zhao, Y. Chen, R. Liu, M. Wu, and W. Xiong, "Monitoring strategy for relay incentive mechanism in cooperative communication networks," *Computers & Electrical Engineering*, vol. 60, pp. 14–29, 2017.

[33] J. N. Laneman and G. W. Wornell, "Distributed space-time-coded protocols for exploiting cooperative diversity in wireless networks," *IEEE Transactions on Information Theory*, vol. 49, no. 10, pp. 2415–2425, 2003.

[34] R. Gibbons, "Incentives between firms (and within)," *Management Science*, vol. 51, no. 1, pp. 2–17, 2005.

[35] S. Boyd and L. Vandenberghe, *Convex Optimization*, Cambridge University Press, Cambridge, UK, 2004.